Measurement of MHD Turbulence Properties by Synchrotron Radiation Techniques

Jian-Fu Zhang[1,2]* and Ru-Yue Wang[1]

[1]Department of Physics, Xiangtan University, Xiangtan, China, [2]Key Laboratory of Stars and Interstellar Medium, Xiangtan University, Xiangtan, China

It is well known that magnetohydrodynamic (MHD) turbulence is ubiquitous *in astrophysical environments*. The correct understanding of the fundamental properties of MHD turbulence is a pre-requisite for revealing many key astrophysical processes. The development of observation-based measurement techniques has significantly promoted MHD turbulence theory and its implications in astrophysics. After describing the modern understanding of MHD turbulence based on theoretical analysis and direct numerical simulations, we review recent developments related to synchrotron fluctuation techniques. Specifically, we comment on the validation of synchrotron fluctuation techniques and the measurement performance of several properties of magnetic turbulence based on data cubes from MHD turbulence simulations and observations. Furthermore, we propose to strengthen the studies of the magnetization and 3D magnetic field structure's measurements of interstellar turbulence. At the same time, we also discuss the prospects of new techniques for measuring magnetic field properties and understanding astrophysical processes, using a large number of data cubes from the Low-Frequency Array (LOFAR) and the Square Kilometre Array (SKA).

Keywords: magnetohydrodynamic turbulence, polarization radiation, interstellar magnetic fields, statistic methods, magnetic fields

1 INTRODUCTION

Turbulence is ubiquitous in our universe. As is perceived in everyday life, the movement of the fluid leads to the development of hydrodynamic turbulence. Unlike our terrestrial world, conductive fluids in astrophysics naturally induce magnetic field fluctuations leading to MHD turbulence due to the presence of almost all materials in an ionization plasma state. The self-similarity over a large dynamical range of MHD turbulence in astronomical environments has been well confirmed by observations, as shown by the power-law spectrum of interstellar electron density fluctuations on the plane of the sky (Armstrong et al., 1995; Chepurnov and Lazarian, 2010). In addition, the presence of MHD turbulence has been also pointed out by observations that are as far as in galaxy clusters (Zhuravleva et al., 2019) as well as by *in situ* direct measurements in the local solar wind (Bruno and Carbone, 2013).

It is known that MHD turbulence plays an important role in many critical astrophysical processes, such as star formation (Mac Low and Klessen, 2004; McKee and Ostriker 2007; Ostriker, 2009; *Dib et al., 2010*; Crutcher, 2012), magnetic reconnection (Lazarian and Vishniac, 1999, henceforth LV99 Lazarian et al., 2020), magnetic field amplification (Federrath, 2016), cosmic ray

acceleration (Gaches et al., 2021; Zhang and Xiang, 2021) and diffusion (Yan and Lazarian, 2008; Xu and Lazarian, 2018; Lazarian and Xu, 2021; Fornieri et al., 2021, for a comprehensive numerical study), and heat conduction in galaxy clusters (Yuan et al., 2015; Bu et al., 2016). Naturally, a thorough understanding of MHD turbulence is essential in order to better describe a large number of astrophysical processes that operate over a large number of physical scales.

MHD turbulence with the nonlinear complexity generally exhibits diverse properties at a microscopic plasma level, but it shows regularity behind chaotic phenomena for turbulent fluctuations and allows a statistical description at a macroscopic level (Biskamp, 2003). Taking statistical description into account, commonly used methods are the power spectrum, the correlation and structure functions (see Monin and Yaglom (1975) for an old book; *Boldyrev et al., 2002a*; *Boldyrev et al., 2002b*), by which one mostly considers volume and time averaging of physical variables to implement the statistical ensemble measurements of turbulence. In addition, the delta-variance spectrum (Stutzki et al., 1998; Dib et al., 2021), as another manifestation of the power spectrum, has been used to characterize turbulence properties.

In recent years, numerical *simulations* or *experiments* combined *with analytical theory* have significantly promoted the study of MHD turbulence (Goldreich and Sridhar, 1995, thereafter GS95; LV99; Cho and Lazarian, 2002; Kowal and Lazarian, 2010; Beresnyak 2017). In particular, *the numerical experiments are* gradually alleviating the gap between the realistic MHD turbulence physics and the *analytical* theory. However, due to the large-scale characteristics inherent in astrophysical systems resulting in a high Reynolds number $R_e > 10^{10}$, it is challenging to simulate a realistic astrophysical environment. The currently available 3D MHD simulations are limited by the Reynolds number of about $R_e \simeq 10^5$ (e.g., Beresnyak, 2019). Therefore, a new observation-based research perspective is needed to break the bottleneck of the direct numerical simulation.

In addition to the study of electron density information, there are two additional sources of information regarding MHD turbulence in astrophysics: turbulent velocity and magnetic fields. The former can be retrieved from spectrometric observations of emission lines (e.g., Lazarian et al., 2002; Lazarian and Pogosyan, 2004), while the latter, by radio observations (Gaensler et al., 2011; Lazarian and Pogosyan, 2012; Lazarian and Pogosyan, 2016, hereafter, LP12 and LP16). The main purpose of this article is to review the progress made in measuring the fundamental properties of MHD turbulence using the radio synchrotron radiation method.

Section 2 describes the fundamentals of MHD turbulence theory necessary to understand what MHD turbulence is and develop magnetic field measurement techniques. In **Section 3**, we provide some basic formulae of synchrotron radiative processes in MHD turbulence. **Section 4** presents various statistical techniques that are being currently developed, the feasibility of which is tested using synthetic, realistic simulation and observational data in **Section 5**. Finally, we give a discussion in **Section 6**.

2 FUNDAMENTALS OF MHD TURBULENCE THEORY

2.1 Turbulence Driving Mechanism
The turbulence energy source driving varies with different astrophysical environments. Here, to simplify considerations, we divide the driving sources into two categories: external and internal driving mechanisms. The former has been considered as a common way for turbulence driving in the simulations of interstellar turbulence, due to the convenience of setting external forces. The most typical cases are supernova explosions in ISM (Spitzer Jr, 1978; *Dib et al., 2006*; Ostriker, 2009; Chamandy and Shukurov, 2020), merger events and active galactic nuclei (AGN) outflows in the intercluster medium (Chandran, 2005; Subramanian et al., 2006; Lazarian et al., 2020) and outflow in molecular clouds (Carroll et al., 2009), and young stellar objects (Federrath, 2016). In contrast, the latter is also accepted generally, such as magnetic reconnection driving/mediating turbulence in various regimes (Huang and Bhattacharjee, 2016; Cerri and Califano, 2017; Franci et al., 2017; Kowal et al., 2017; Dong et al., 2018), the magneto-rotational instability-generated turbulence (Sellwood and Balbus, 1999; Gardiner and Stone, 2005; Fromang, 2013; Kunz et al., 2016; Riols et al., 2017; Zhdankin et al., 2017). Indeed, for realistic astrophysical processes such as molecular clouds and supernovae, their drivings may be involved in internal and external mechanisms simultaneously.

Sometimes the complexity of turbulent driving is manifested by the coexistence of multiple driving mechanisms in the same environment. One of the most classic cases is the driving process in the ISM, where various drivers may occur simultaneously: expanding shells and gravitational instability at about 1,000 pc scales arising from galaxy mergers; expanding shells, MRI and cloud collisions at about 100 pc scales from supernova explosion; and stellar feedback at 10-pc to sub-pc scales by outflow. In the turbulence research community, for simplicity, one usually uses external driving with the solenoidal or compressible approach, which is more effective at limited numerical resolution. In recent years, internal driving mechanisms have gradually become the focus of research, but only at the cost of expensive numerical resources (Beresnyak, 2017; Kowal et al., 2017).

2.2 Basic Properties of MHD Turbulence
In the spirit of understanding the nature of turbulence from first principles, we here provide the visco-resistive equations that govern the evolution of magnetized plasma as follows[1]:

$$\frac{\partial \rho}{\partial t} + \nabla \cdot (\rho \mathbf{v}) = 0, \tag{1}$$

---

[1]These equations can be applied to describe the plasma dynamics in the case of the long wavelengths and low frequencies with respect to plasma characteristic scales and frequencies, and the associated plasma approximations such as quasi neutrality, no displacement current in Ampére's law because of non-relativistic limit, as well as resistive Ohm's law (refer to Chapter 3 of the work of Krall and Trivelpiece (1973) for further details).

$$\rho\left(\frac{\partial}{\partial t} + \mathbf{u}\cdot\nabla\right)\mathbf{u} = \frac{\mathbf{j}\times\mathbf{B}}{c} - \nabla p_{\mathrm{g}} + \rho\nu\nabla^2\mathbf{u}, \qquad (2)$$

$$\frac{\partial p_{\mathrm{g}}}{\partial t} + \mathbf{u}\cdot\nabla p_{\mathrm{g}} + \Gamma p_{\mathrm{g}}\nabla\cdot\mathbf{u} = 0, \qquad (3)$$

$$\frac{\partial\mathbf{B}}{\partial t} - \nabla\times(\mathbf{u}\times\mathbf{B}) = \eta\nabla^2\mathbf{B}, \qquad (4)$$

$$\nabla\cdot\mathbf{B} = 0, \qquad (5)$$

describing the continuity, **Eq 1**, the momentum conservation, **Eq 2**, the adiabatic invariance, **Eq 3**, the magnetic induction, **Eq 4**, and the divergence of magnetic field, **Eq 5**, respectively. Here, $p_{\mathrm{g}} = c_{\mathrm{s}}^2\rho$ is the gas pressure, $c_{\mathrm{s}} = \sqrt{\Gamma p_{\mathrm{g}}/\rho}$ the speed of sound, t the evolution time of the fluid, ν the kinematic viscosity, $\eta = c^2/(4\pi\sigma)$ the magnetic diffusivity, σ the conductivity, and Γ the adiabatic index. Other physical quantities have their usual meanings. The interaction of plasma fluids and magnetic field was formulized in the aforementioned equations, by which a series of physical quantities characterizing the properties of the MHD turbulence can be better understood.

Let us replace the operator ∇ by ∇/L and set $\mathbf{u} = u\tilde{\mathbf{u}} = L/t\tilde{\mathbf{u}}$ in **Eq 2** and $\mathbf{B} = B\tilde{\mathbf{B}}$ in **Eq 4**, where L is the characteristic scale length at the typical velocity u, as well as $\tilde{\mathbf{u}}$ and $\tilde{\mathbf{B}}$ are dimensionless. After a simple analytical derivation (including only the viscosity term in **Eq (2)**), we obtain

$$\frac{\partial\tilde{\mathbf{u}}}{\partial t} + \tilde{\mathbf{u}}\cdot\nabla\tilde{\mathbf{u}} = \frac{\nu}{uL}\nabla^2\tilde{\mathbf{u}}, \qquad (6)$$

$$\frac{\partial\tilde{\mathbf{B}}}{\partial t} - \nabla\times(\tilde{\mathbf{u}}\times\tilde{\mathbf{B}}) = \frac{\eta}{Lu}\nabla^2\tilde{\mathbf{B}}. \qquad (7)$$

Through the coefficients of the equations, we define two dimensionless physical quantities

$$R_{\mathrm{e}} = \frac{Lu}{\nu}, \quad R_{\mathrm{m}} = \frac{Lu}{\eta}, \qquad (8)$$

where R_{e} is the kinetic Reynolds number characterizing the ratio of the viscous timescale to the advection timescale, and R_{m} is the magnetic Reynolds number denoting the ratio of resistive diffusion timescale to the advection timescale. Considering the temperature $T \simeq 10^4\mathrm{K}$ related to $\eta \simeq 0.42\times10^7 T_{\mathrm{eV}}^{-3/2}\,\mathrm{cm}^2/s$, the scale length $L \simeq 1$ pc, and the velocity $u \simeq 1$ km/s, one can obtain a large $R_{\mathrm{m}} \simeq 10^{16}$ as an example of turbulence setting (e.g., Brandenburg and Subramanian, 2005). The relative dominance between the kinematic viscosity and magnetic diffusivity is described by the magnetic Prandtl number:

$$P_{\mathrm{r}} = \frac{R_{\mathrm{m}}}{R_{\mathrm{e}}} = \frac{\nu}{\eta}. \qquad (9)$$

Similarly, combining the adiabatic invariance, **Eq 3** and momentum conservation, **Eq 2**, one can obtain the sonic Mach number (Biskamp, 2003 for a detailed derivation)

$$M_{\mathrm{s}} = u/c_{\mathrm{s}}, \qquad (10)$$

for the high-β plasma case. This parameter can be used to describe the information of compressibility of MHD turbulence. For the low-β plasma case, the momentum conservation **Eq 2** is dominated by the magnetic pressure. On multiplying **Eq 2** by $\mathbf{u} = u\tilde{\mathbf{u}}$, the quantity characterizing the magnetization strength is called the Alfvénic Mach number

$$M_{\mathrm{A}} = u/V_{\mathrm{A}}, \qquad (11)$$

where $V_{\mathrm{A}} = B/\sqrt{4\pi\rho}$ is the Alfvénic velocity.

Considering current density $(\nabla\times\mathbf{B} = \frac{4\pi}{c}\mathbf{j})$ related to the magnetic field by Ampere's law, the Lorentz force can be written in the following form:

$$\frac{\mathbf{j}\times\mathbf{B}}{c} = \frac{(\mathbf{B}\cdot\nabla)\mathbf{B}}{4\pi} - \nabla\frac{\mathbf{B}^2}{8\pi}, \qquad (12)$$

where the first term on the right-hand side describes the magnetic tension force and the second term describes the magnetic pressure force. The plasma parameter β, denoting the ratio of gas pressure to magnetic one, is defined as

$$\beta = \frac{p_{\mathrm{g}}}{B^2/8\pi}, \qquad (13)$$

which can be rewritten as

$$\beta = \frac{2M_{\mathrm{A}}^2}{M_{\mathrm{s}}^2}, \qquad (14)$$

with the sonic and Alfvén Mach numbers.

As for the description of the properties of helicity *in* MHD turbulence, one can introduce another two quantities termed as the magnetic helicity and cross helicity, which are, respectively, written as

$$H^M = \int_V \mathbf{A}\cdot\mathbf{B}\,dV, \qquad (15)$$

$$H^C = \int_V \mathbf{u}\cdot\mathbf{B}\,dV. \qquad (16)$$

Here, $\mathbf{A}$ is the vector potential with $\mathbf{B} = \nabla\times\mathbf{A}$. The former can measure the twist and linkage of the magnetic field lines, and the latter can reflect the overall correlation of magnetic and velocity fields (Falgarone and Passot, 2003).

2.3 Cascade Processes of MHD Turbulence

2.3.1 Power-Law Scaling of Turbulence Cascade

The pioneering work regarding incompressible hydrodynamic turbulence (Kolmogorov, 1941, henceforth K41) demonstrated that the energy is injected at a large scale (called the injection scale) and dissipated at small scales (the dissipation scale). The range between these two scales is called the inertial range, where the energy cascades from the injection scale to the dissipation scale with negligible energy losses, that is, the energy transfer rate in this range keeps a constant,

$$\epsilon \approx u_l^2/t_{\mathrm{cas}} = const., \qquad (17)$$

where u_l is a characteristic velocity and $t_{cas} = l/u_l$ is the cascading timescale. This expression indirectly reflects the relationship between velocity u_l of fluid elements and their scales l, namely $u_l \propto (\epsilon l)^{1/3}$. Therefore, we have the well-known Kolmogorov 1D spectrum

$$E(k) \sim \epsilon^{2/3} k^{-5/3}, \tag{18}$$

where k is the wave number. Alternatively, the 3D spectrum is expressed as

$$E_{3D}(k) \sim k^{-11/3}. \tag{19}$$

It is noted that this 3D spectrum can be transformed into the 1D one by the transformation of the volume element $d^3k \sim k^2 dk$, i.e., $E(k) \sim k^2 E_{3D}(k) \sim k^{-5/3}$.

For incompressible magnetic turbulence, two classical works (Iroshnikov, 1963; Kraichnan, 1965, henceforth IK) introduced nonlinear energy models to study the power-law scaling from turbulence cascade. Different from the K41 energy cascade by the interaction of eddies, it is considered that the energy was transferred via the Alfvén waves along the local magnetic field. The relation between the velocity and scale is expressed as $u_l \propto (\epsilon V_A l)^{1/4}$ after considering the influence of the magnetic field. The power spectrum in the IK theory is

$$E(k) \sim (\epsilon V_A)^{1/2} k^{-3/2} \tag{20}$$

in the inertial range. Although this model considered the role of the magnetic field, it ignored a critical issue that turbulence should be anisotropic in the presence of the magnetic field. This limitation was pointed out in later studies (Montgomery, 1982; Shebalin et al., 1983).

With the anisotropy due to turbulent magnetic fields, GS95 studied the nonlinear energy cascade of incompressible and strong MHD turbulence. They predicted that the motions of eddies perpendicular to the magnetic field have similar properties to Kolmogorov turbulence, i.e., $v_\perp \propto (\epsilon l_\perp)^{1/3}$. The resulting Kolmogorov-like energy spectra are given by

$$E(k_\perp) \propto \epsilon^{2/3} k_\perp^{-5/3}, \tag{21}$$

where $k_\perp$ represents the wave-vector component perpendicular to the magnetic field. Notice that the magnetic field in the original article refers to the global frame of reference which has been corrected as the local frame of reference by later intensive studies (LV99; Cho and Vishniac, 2000; Maron and Goldreich, 2001; Cho and Lazarian, 2002; Cho and Lazarian, 2003, henceforth CL02; 2003, henceforth CL03). In particular, the LV99 theory pointed out that the reconnection of turbulent magnetic fields takes place within the eddy turnover time and the motions of eddies perpendicular to the magnetic field are not controlled by the magnetic field tension. The magnetic field here refers to the local magnetic field around the eddies.

Besides, for the weak MHD turbulence, the energy transfer rate is expressed as $\epsilon \propto (V_L^4 l_\parallel / V_A l_\perp^2)$, resulting in $v_l \propto V_L (l_\perp/L_{in})^{1/2}$. Thus, the power spectrum of weak turbulence follows (LV99; Galtier et al., 2000)

$$E(k_\perp) \sim k_\perp^{-2}. \tag{22}$$

2.3.2 Anisotropy

Except for the prediction of the exponent of $-5/3$ in the perpendicular direction mentioned previously, another important contribution of the GS95 theory is the prediction of scale-dependent anisotropy. They assumed that the relative motion perpendicular and parallel to the magnetic field is described by the critical balance condition, namely, $l_\perp^{-1} v_\perp \sim l_\parallel^{-1} V_A$, where $v_\perp$ is fluctuation velocity of turbulence at the scale $l_\perp$, $l_\parallel$ and $l_\perp$ represent the scales parallel and perpendicular to the magnetic field, respectively. Based on the critical balance condition and the relation of $v_\perp \propto (\epsilon l_\perp)^{1/3}$, two scales are related by

$$l_\parallel \sim V_A \epsilon^{-1/3} l_\perp^{2/3}, \tag{23}$$

which is the so-called scale-dependent anisotropy theory. This implies that the smaller the scale, the larger the anisotropy. Note that this anisotropic relationship holds in the local frame of reference rather than in the global frame of reference. As for the latter, the anisotropy is scale-independent and is determined by the anisotropy of the largest eddies (CL03).

It should be stressed that GS95 focused on trans-Alfvénic turbulence, i.e., $M_A \approx 1$, with the turbulence kinetic energy equal to the magnetic energy. Later, the theory was generalized to sub-Alfvénic $M_A < 1$ and super-Alfvénic $M_A > 1$ cases, respectively (LV99; Lazarian, 2006). When the turbulence is driven with the injection velocity V_L less than V_A at the injection scale L_{in}, it initially undergoes a weak turbulence cascade process with $v_l \propto l_\perp^{1/2}$, where the parallel scale $l_\parallel$ does not change (LV99; Galtier et al., 2000). With the intensification of the interaction of wave packets, the turbulence changes to strong turbulence at the transition scale $L_{tr} = L_{in} M_A^2$ and continues up to the dissipative scale L_{dis}. In the inertial range, the scales perpendicular and parallel to the magnetic field have the following relationship:

$$l_\parallel \approx L_{in}^{1/3} l_\perp^{2/3} M_A^{-4/3}. \tag{24}$$

Compared with the trans-Alfvénic turbulence, this relationship has an additional factor related to the magnetization $M_A^{-4/3}$. In addition, the turbulent velocity is written as

$$v_l \approx V_L \left(\frac{l_\perp}{L_{in}} \right)^{1/3} M_A^{1/3}, \tag{25}$$

which still follows the Kolmogorov-type cascade, i.e., $v_l \propto l_\perp^{1/3}$.

In the case of the super-Alfvénic turbulence, there is almost no constraint of the magnetic field at the injection scale L_{in}, so the turbulence follows the law of hydrodynamic turbulence. With the development of turbulence, it experiences a transition from hydrodynamic turbulence to MHD one at the transition scale $L_A = L_{in} M_A^{-3}$. In the inertial range from L_A to L_{dis}, the turbulence again exhibits an anisotropy consistent with the GS95 theory, with the scale relation of

$$l_\parallel \approx L_{in}^{1/3} l_\perp^{2/3} M_A^{-1} \tag{26}$$

and the velocity relation of

$$v_l \approx V_L \left(\frac{l_\perp}{L_{in}} \right)^{1/3}. \tag{27}$$

In the strongly turbulent region, the scale-dependent anisotropy becomes more significant as the scale decreases.

2.4 Compressibility of MHD Turbulence

Compressibility is an important addition to the MHD turbulence theory. In fact, in a real astrophysical environment such as a molecular cloud, the MHD turbulence is essentially compressible and is composed of three plasma modes, i.e., Alfvén, slow, and fast modes. The idea of the decomposition of MHD turbulence into individual modes was originally formulated in Dobrowolny et al. (1980), where they mainly dealt with small amplitude perturbations in incompressible MHD turbulence.

The actual decomposition in a numerical simulation has been implemented using Fourier transformation (CL02; CL03). Covering the gas pressure-dominated and magnetic pressure-dominated turbulence regimes, they revealed the spectrum and anisotropy in the compressible MHD turbulence. Typically, the Alfvén mode in the high- and low-β regimes follows the scaling slope and scale-dependent anisotropy of GS95.

$$E^A(k) \propto k_\perp^{-5/3}, \quad k_\parallel \propto k_\perp^{2/3}. \tag{28}$$

The slow mode, as a passive mode, is dominated by the Alfvén mode, and has properties similar to those of the Alfvén mode:

$$E^s(k) \propto k_\perp^{-5/3}, \quad k_\parallel \propto k_\perp^{2/3}. \tag{29}$$

The fast mode, different from the Alfvén and slow modes, possesses isotropic properties similar to acoustic turbulence, with the following scaling relations:

$$E^f(k) \propto k^{-3/2}, \quad k_\parallel \propto k_\perp. \tag{30}$$

Later, Kowal and Lazarian (2010) advanced the studies on mode decomposition using a wavelet method to treat large amplitude perturbations. This method enables us to trace the direction of the local magnetic field and has significant advantages over the Fourier transform done in the frame of reference of the mean magnetic field.

2.5 Controversy

To explain the numerical simulations in Maron and Goldreich (2001), several studies that have attracted community attention proposed a particular process termed as dynamical alignment to modify the GS95 spectrum from $k^{-5/3}$ to $k^{-3/2}$ (Boldyrev, 2005; Boldyrev, 2006; Mason et al., 2006). At present, there are numerical results that are compatible with a dynamic alignment model (e.g., Chandran et al., 2015). Moreover, solar-wind observations seem to find some scale-dependent alignment (e.g., Wicks et al., 2013) or the emergence of three-dimensional anisotropy (e.g., Chen et al., 2011) which would also point toward a scale-dependent alignment of some sort (see also Wang T et al., 2020 for similar findings from the end of the MHD cascade to the kinetic scales).

At scales close to the dissipation scale, another modification of the GS95 theory was proposed by Mallet and Schekochihin (2017) for their intermittency model and Mallet et al. (2017) for their reconnection-mediated turbulence model (see also Loureiro and Boldyrev, 2017), the testing/confirming of which is difficult due to current limitations in computational abilities.

However, the anisotropy predicted in Bolryrev's work is inconsistent with some recent numerical simulations (Beresnyak, 2019; Beresnyak and Lazarian, 2019). Many studies claimed that the deviation from the spectral index -5/3 is transient, namely, localized in the vicinity of the injection scale, and does not extend to the whole inertial range (Beresnyak and Lazarian, 2010; Beresnyak, 2013; Beresnyak, 2014). To the best of my knowledge, this issue is still open. Anyway, the current attempts still do not change the paradigm of the modern MHD turbulence theory.

Synchrotron fluctuation techniques reviewed in this article are developed closely based on the modern understanding of MHD turbulence theory (e.g., GS95; LV99; CL02) without more concern for its controversial appearance. Fortunately, modifications attempted to the fundamental theory are not expected to seriously affect the measurement of the techniques. This is because the development of measurement techniques is independent of a specific scaling slope of turbulence and is constrained in the strongly turbulent range, while modifications to turbulence theory focus on the driving or dissipation scale.

3 SYNCHROTRON RADIATIVE PROCESSES IN MHD TURBULENCE

Magnetic field and relativistic electrons, as two key factors, play a decisive role in emitting synchrotron radiation (Ginzburg and Syrovatskii, 1965; Ginzburg, 1981). Assume that relativistic electrons display a power-law spectrum

$$N(E)\,dE = KE^{-p}\,dE, \tag{31}$$

where N represents the number density of relativistic electrons with the energy between E and $E + dE$, K the normalization constant, and p spectral index of the electrons. In an environment containing regular and random magnetic fields, synchrotron emissivity can be expressed as the combination of homogeneous (j_h) and random (j_r) parts (Crusius and Schlickeiser, 1986)

$$j(\nu,\theta) = \chi j_\mathrm{h}(\nu,\theta) + \frac{1}{2}\left(1-\chi\right) j_\mathrm{r}(\nu), \tag{32}$$

where χ and $1-\chi$ are the percentage of homogeneous and random parts, respectively. θ is the angle between field lines and the direction of emission, and the factor $\frac{1}{2}$ denotes half of the power $j_\mathrm{r}(\nu)$ measured in the each of two polarization directions for turbulent magnetic fields.

3.1 Radiation in Homogeneous Magnetic Field

In a completely homogeneous field, the synchrotron emissivity of relativistic electrons is expressed by (Ginzburg and Syrovatskii, 1965)

$$j_\mathrm{h}(\nu,\theta) = \int dE N(E)\,\mathcal{F}(E,\nu,\theta). \tag{33}$$

The integrand $\mathcal{F}$, representing the power per frequency unit emitted by a single electron of given energy and pitch angle, is given by (see Rybicki and Lightman, 1979 for more details on the derivation)

$$\mathcal{F}(E, v, \theta) = \frac{\sqrt{3}e^3 B \sin\theta}{m_e c^2}\left[\frac{v}{v_c}\int_{v/v_c}^{\infty} K_{5/3}(t)\,dt\right], \quad (34)$$

where $K_{5/3}(t)$ is the modified Bessel function of order $5/3$, $f\left(\frac{v}{v_c}\right) = \frac{v}{v_c}\int_{v/v_c}^{\infty} K_{5/3}(t)dt$ is often referred to as a kernel function, and $v_c = 3E^2 eB\sin\theta/4\pi m_e^3 c^5$ is a characteristic frequency of synchrotron emission.

The power per frequency of a single electron, $\mathcal{F}$, is divided into the perpendicular and parallel components with respect to the magnetic field B (Rybicki and Lightman, 1979).

$$\mathcal{F}_{\perp}(E, v, \theta) = \frac{\sqrt{3}e^3 B \sin\theta}{2m_e c^2}\left[f\left(\frac{v}{v_c}\right) + g\left(\frac{v}{v_c}\right)\right], \quad (35)$$

$$\mathcal{F}_{\parallel}(E, v, \theta) = \frac{\sqrt{3}e^3 B \sin\theta}{2m_e c^2}\left[f\left(\frac{v}{v_c}\right) - g\left(\frac{v}{v_c}\right)\right], \quad (36)$$

where $g(v/v_c) = \frac{v}{v_c}K_{\frac{2}{3}}\left(\frac{v}{v_c}\right)$ and $K_{\frac{2}{3}}$ is the modified Bessel function of order $2/3$. As a result, the degree of linear polarization can be calculated by

$$\Pi(v) = \frac{\mathcal{F}_{\perp} - \mathcal{F}_{\parallel}}{\mathcal{F}_{\perp} + \mathcal{F}_{\parallel}} = \frac{g(v/v_c)}{f(v/v_c)} \quad (37)$$

for a single electron radiation. Replacing $\mathcal{F}$ in **Eq 33** with $\mathcal{F}_{\parallel}$ or $\mathcal{F}_{\perp}$, we can obtain the perpendicular ($j_{\perp}$) and parallel ($j_{\parallel}$) components of synchrotron emissivity for electron populations. Hence, we have the degree of linear polarization for the electron populations.

$$\Pi(v) = \frac{j_{\perp} - j_{\parallel}}{j_{\perp} + j_{\parallel}}. \quad (38)$$

After integration, the total emissivity (**Eq 33**) can be simplified as

$$j_h(v, \theta) \propto (B_{\perp})^{(p+1)/2} v^{-(p-1)/2}, \quad (39)$$

where the spectral index of photons is $\alpha = \frac{p-1}{2}$ and $B_{\perp} = B\sin\theta$.

3.2 Radiation in Random Magnetic Field

In a completely random field, the calculation of synchrotron emissivity will be more complex compared to a completely homogeneous field, due to the presence of a stochastic direction. The synchrotron emissivity is formulated as (Crusius and Schlickeiser, 1986)

$$j_r(v) = \frac{1}{4\pi}\int_0^{2\pi} d\varphi \int_0^{\pi} d\theta \sin\theta j_h(v, \theta), \quad (40)$$

by averaging the total spontaneously emitted power for the homogeneous field $j_h(v, \theta)$ over all possible values of the polar (θ) and azimuthal (φ) angles. This equation implies that randomness

of the magnetic field is maintained ranging from the Larmor radii of the radiating electrons to the size of the emitting source.

Defining $x = v \sin\theta/v_c$, **Eq 40** can be rewritten as

$$j_r(v) \propto B \int_0^{\infty} dE N(E) R(x), \quad (41)$$

where $x = \frac{v}{(c_1 B E^2)}$, $c_1 = \frac{3e}{4\pi m_e^3 c^5}$ and $R(x) = \frac{x}{2}\int_0^{\pi} d\theta \sin\theta \int_{x/\sin\theta}^{\infty} K_{5/3}(t)dt$ is associated with the Bessel function of order $5/3$. The analytical results demonstrated that j_r has the same power–law relation for frequency as that of j_h (Crusius and Schlickeiser, 1986). Different from the situation of homogeneous field, j_r is related to the total magnetic field strength B and not just its perpendicular component $B_{\perp}$ in j_h expression.

3.3 Synchrotron Self-Absorption

When involving in the synchrotron self-absorption, one can adopt **Eq 34** to obtain the following the self-absorption coefficient:

$$\kappa(v, \theta) = \frac{c^2}{8\pi v^2}\int E^2 \frac{d}{dE}\left(\frac{N(E)}{E^2}\right)\mathcal{F}(E, v, \theta)\,dE. \quad (42)$$

We can, thus, write total radiation intensity by the radiative transfer equation

$$I(v) = \frac{j}{\kappa}\left(1 - e^{-\tau}\right), \quad (43)$$

where $\tau = \kappa\ell$ is the absorption optical depth, and ℓ is the size of the emitting region.

For the electrons with a power-law distribution, the absorption coefficient can be reduced to

$$\kappa(v, \theta) = \frac{p + 10/3}{p + 2}\mu(v, \theta)$$
$$= G(p)\frac{e^3}{2\pi m_e}\left(\frac{3e}{2\pi m_e^3 c^5}\right)^{p/2} K (B\sin\theta)^{(p+2)/2} v^{-(p+4)/2}, \quad (44)$$

where $\mu(v, \theta) = \frac{p+2}{p+10/3}\kappa(v, \theta)$, and the coefficient $G(p) = \frac{\sqrt{3}}{4}\Gamma\left(\frac{3p+2}{12}\right)\Gamma\left(\frac{3p+22}{12}\right)$ is only associated with the electron exponent.

To obtain polarization properties, we herein introduce the following coefficients in two mutually perpendicular directions:

$$\kappa_{\perp}(v, \theta) = \kappa(v, \theta) + \mu(v, \theta), \quad (45)$$

$$\kappa_{\parallel}(v, \theta) = \kappa(v, \theta) - \mu(v, \theta). \quad (46)$$

By adapting **Eq 43**, we have radiation intensity components

$$I_{\perp}(v) = \frac{j_{\perp}}{\kappa_{\perp}}\left(1 - e^{-\kappa_{\perp}\ell}\right), \quad (47)$$

$$I_{\parallel}(v) = \frac{j_{\parallel}}{\kappa_{\parallel}}\left(1 - e^{-\kappa_{\parallel}\ell}\right). \quad (48)$$

As for an optically thin medium, i.e., $\kappa_{\perp,\parallel}\ell \ll 1$, the degree of linear polarization is consistent with **Eq. 38**. In the case of optically thick medium, i.e., $\kappa_{\perp,\parallel}\ell \gg 1$,

$$\Pi(v) = \frac{j_{\perp}/\kappa_{\perp} - j_{\parallel}/\kappa_{\parallel}}{j_{\perp}/\kappa_{\perp} + j_{\parallel}/\kappa_{\parallel}} \quad (49)$$

can be used to calculate the degree of linear polarization.

4 STATISTICS OF SYNCHROTRON FLUCTUATIONS

On the basis of synchrotron emissivity in **Section 3**, we can obtain the observable synchrotron intensity (I) and polarization intensity (P) by integrating along the line of sight (Burn, 1966; Waelkens et al., 2009).

$$I(\mathbf{X}) = \int_0^L (j_\perp + j_\parallel)\, dz, \tag{50}$$

$$\mathbf{P}(\mathbf{X}, \lambda^2) = \int_0^L (j_\perp - j_\parallel)\, e^{2i\psi(\mathbf{X},z)}\, dz, \tag{51}$$

where L is the spatial scale of radiative propagation, $\mathbf{X}$ is a 2D vector on the plane of the sky, and z is the distance variable along the line of sight. The phase (polarization) angle $\psi(\mathbf{X}, z) = \psi_0 + \lambda^2 \Phi$ is associated with the intrinsic polarization angle ψ_0 and the Faraday rotation measure Φ. This is expressed as

$$\Phi(\mathbf{X}, z) \propto \int_0^z n_e(\mathbf{X}, z')\, B_\parallel(\mathbf{X}, z')\, dz', \tag{52}$$

where n_e is the thermal electron density and $B_\parallel$ is the magnetic field parallel component along the line of sight. Defining the intrinsic polarization intensity density as $\mathbf{P_i} = \mathbf{Q_i} + i\mathbf{U_i}$ which is independent of wavelengths (this simplification does not affect the statistical results, as verified in Zhang et al., 2018), we can write the polarization intensity $\mathbf{P} = \mathbf{Q} + i\mathbf{U}$ as

$$\mathbf{P}(\mathbf{X}, \lambda^2) = \int_0^L dz\, \mathbf{P_i}(\mathbf{X}, z)\, e^{2i\lambda^2 \Phi(\mathbf{X},z)}. \tag{53}$$

4.1 Correlation Analysis of Synchrotron Fluctuations

According to the commonly used method of correlation analysis, the two-point correlation of the polarized intensities can be expressed as (LP16)

$$\langle \mathbf{P}(\mathbf{X_1}, \lambda_1^2)\, \mathbf{P}^*(\mathbf{X_2}, \lambda_2^2) \rangle = \int_0^L dz_1 \int_0^L dz_2$$
$$\langle \mathbf{P_i}(\mathbf{X_1}, z_1)\, \mathbf{P_i}^*(\mathbf{X_2}, z_2)\, e^{2i\left(\lambda_1^2 \Phi(\mathbf{X_1}, z_1) - \lambda_2^2 \Phi(\mathbf{X_2}, z_2)\right)} \rangle, \tag{54}$$

where $\mathbf{P}*$ denotes the conjugate of the polarization intensity, $\mathbf{X_1}$ and $\mathbf{X_2}$ represent two different spatial positions on the plane of the sky, and λ_1 and λ_2 correspond to two wavelengths. **Eq 54** can not only characterize the correlation of the spatial separation but also the dispersion of frequencies. Based on this, LP16 proposed two techniques, namely the polarization spatial analysis (PSA) and the polarization frequency analysis (PFA).

In analogy with the velocity channel analysis (VCA) technique (Lazarian et al., 2002), the PSA correlates the polarization signal at different spatial points of the position–position frequency (PPF) space that has similarities with the position–position

volume (PPV) space. At a fixed wavelength, the PSA can be expressed as

$$\langle \mathbf{P}(\mathbf{X_1})\, \mathbf{P}^*(\mathbf{X_2}) \rangle = \int_0^L dz_1 \int_0^L dz_2\, e^{2i\overline{\phi}\lambda^2(z_1 - z_2)}$$
$$\times \langle \mathbf{P_i}(\mathbf{X_1}, z_1)\, \mathbf{P_i}^*(\mathbf{X_2}, z_2) \rangle$$
$$\times e^{-2\lambda^4}\langle(\triangle\Phi(\mathbf{X_1}, z_1) - \triangle\Phi(\mathbf{X_2}, z_2))^2\rangle, \tag{55}$$

where $\overline{\phi}$ is the mean Faraday rotation measure density and $\Delta\Phi$ is the fluctuation of Faraday rotation measure. This represents the correlation of polarization intensity as a function of spatial separation $\mathbf{R} = \mathbf{X_2} - \mathbf{X_1}$ at the same wavelength.

The PFA that is analogous to the velocity coordinate spectrum (VCS) correlates the polarization information along a single line of sight at the same spatial position. At a fixed spatial position, the PFA for different wavelengths is expressed by

$$\langle \mathbf{P}(\lambda_1^2)\, \mathbf{P}^*(\lambda_2^2) \rangle = \int_0^L dz_1 \int_0^L dz_2\, e^{2i\overline{\phi}\left(\lambda_1^2 z_1 - \lambda_2^2 z_2\right)}$$
$$\langle \mathbf{P_i}(z_1)\, \mathbf{P_i}^*(z_2)\, e^{2i\left(\lambda_1^2 \triangle\Phi(z_1) - \lambda_2^2 \triangle\Phi(z_2)\right)} \rangle, \tag{56}$$

which is complementary to the PSA, so this enables a more comprehensive acquisition of the properties of MHD turbulence.

Another important aspect of the development of the synchrotron fluctuation technique is the construction of the statistics of polarization intensity derivative with respect to the squared wavelength λ^2. The correlation statistics of $dP/d\lambda^2$ is formulated as

$$\left\langle \frac{\mathbf{dP}(\mathbf{X_1})}{d\lambda^2} \frac{\mathbf{dP}^*(\mathbf{X_2})}{d\lambda^2} \right\rangle = \int_0^L dz_1 \int_0^L dz_2\, e^{2i\overline{\phi}\lambda^2(z_1 - z_2)}$$
$$\times \langle \mathbf{P_i}(\mathbf{X_1}, z_1)\, \mathbf{P_i}^*(\mathbf{X_2}, z_2)\, \Delta\Phi(\mathbf{X_1}, z_1)$$
$$\times \Delta\Phi(\mathbf{X_2}, z_2)\, e^{-2\lambda^2 i(\Delta\Phi(\mathbf{X_1}, z_1) - \Delta\Phi(\mathbf{X_2}, z_2))} \rangle, \tag{57}$$

which is more sensitive to the fluctuations of Faraday rotation than the polarization intensity correlation given in **Eq 55**. The introduction of this relationship allows for more information such as the spectrum of Faraday rotation to be obtained. In addition to considering the correlation function, one can also use the structure function of polarization intensity to reveal the anisotropy of MHD turbulence (see LP16 for detailed formulation).

4.2 Analysis of Power Spectrum

With the correlation analysis of synchrotron fluctuations, the power spectrum of synchrotron polarization is described through the Fourier transform of the two-point correlation tensor as

$$E_{\mathbf{P}}(\mathbf{K}) = \frac{1}{(2\pi)^2} \int d\mathbf{R}\, e^{-i\mathbf{K}\cdot\mathbf{R}} \langle \mathbf{P}(\mathbf{X_1})\, \mathbf{P}^*(\mathbf{X_2}) \rangle, \tag{58}$$

where $\mathbf{R} = \mathbf{X_1} - \mathbf{X_2} \propto 1/\mathbf{K}$ is the spatial lag vector on the plane of the sky. Similarly, the power spectrum of the polarization derivative with respect to λ^2 can be written as

$$E_{\mathbf{dP}}(\mathbf{K}) = \frac{1}{(2\pi)^2} \int d\mathbf{R}\, e^{-i\mathbf{K}\cdot\mathbf{R}} \left\langle \frac{\mathbf{dP}(\mathbf{X_1})}{d\lambda^2} \frac{\mathbf{dP}^*(\mathbf{X_2})}{d\lambda^2} \right\rangle \tag{59}$$

for analyzing the multi-frequency observations. Once the power spectrum distribution of the observed information is obtained

through the aforementioned two equations, we can obtain the distribution characteristics of turbulent energy in space, and also understand several properties related to turbulence, such as the scaling slope, energy dissipation, and injection scales.

4.3 Analysis of Anisotropy

Following LP12, we can define the normalized correction function for an arbitrary observable F as

$$\xi_F(\mathbf{R}) = \frac{\langle F(\mathbf{X})F(\mathbf{X}+\mathbf{R})\rangle - \langle F(\mathbf{X})\rangle^2}{\langle F(\mathbf{X})^2\rangle - \langle F(\mathbf{X})\rangle^2}, \tag{60}$$

where $\mathbf{X}$ and $\mathbf{R}$ denote a spatial position and a separation between any two points on the plane of the sky, respectively. This is related to the normalized structure function of the observable F

$$\tilde{D}_F = 2\left(1 - \xi_F\right), \tag{61}$$

by which we have a multi-pole expansion

$$\tilde{M}_n(\mathbf{R}) = \frac{1}{2\pi}\int_0^{2\pi} e^{-in\varphi}\tilde{D}_F(\mathbf{R},\varphi)\,d\varphi, \tag{62}$$

where n represents the order of multi-pole and φ is the polar angle. The order of the multi-pole expansion has following meaning: $n = 0$ represents the monopole reflecting the isotropy of statistics, $n = 1$ denotes the dipole which is zero due to the rotational symmetry of the structure function, $n = 2$ is called the quadrupole moment revealing the anisotropy, and $n = 4$ is the octupole moment which has a negligible contribution for the anisotropy. Hence, we define the ratio of the quadrupole moment to the monopole one (termed quadrupole ratio, ref. LP16)

$$\Re_Q = \frac{\tilde{M}_2(\mathbf{R})}{\tilde{M}_0(\mathbf{R})} = \frac{\int_0^{2\pi} e^{-2i\varphi}\tilde{D}_F(\mathbf{R},\varphi)\,d\varphi}{\int_0^{2\pi}\tilde{D}_F(\mathbf{R},\varphi)\,d\varphi} \tag{63}$$

to characterize the degree of anisotropy, and the absolute value of which is called the quadrupole ratio modulus.

Alternatively, the ratio of structure functions in the perpendicular direction to each other can also depict the level of anisotropy and is given by

$$\Re_S = \frac{\langle|F_\parallel(x+R_\parallel)-F_\parallel(x)|^2\rangle}{\langle|F_\perp(y+R_\perp)-F_\perp(y)|^2\rangle}, \tag{64}$$

where $R = (R_\parallel^2 + R_\perp^2)^{1/2}$ is the spatial separation on the plane of the sky. When $\Re_S = 1$, statistics represents an isotropy while any deviation from $\Re_S = 1$ implies an appearance of anisotropy.

4.4 Statistics of Spatial Gradients
Combining the local alignment theory of MHD turbulence (GS95; LV99) with the synchrotron polarization fluctuation predictions (LP16), the gradient techniques were proposed to measure the properties of MHD turbulence (Lazarian et al., 2017; Lazarian and Yuen, 2018a). This is analogous to velocity gradient techniques (González-Casanova and Lazarian, 2017; Yuen and

Lazarian, 2017). The feasibility lies in that magnetic field and velocity fluctuations enter symmetrically, according to the theory of Alfvénic turbulence. In the framework of GS95 MHD turbulence theory, it is expected that the alignment of the magnetic field gradient direction is perpendicular to the local magnetic field direction with the eddies (for other different anisotropy models, the sensitivity to this alignment effect may significantly depend on the scales). Since the synchrotron fluctuations are elongated in the direction of the mean magnetic fields, the magnetic fields can be traced by the direction of the spatial gradient of the observed signal.

When involved in Faraday depolarization of synchrotron radiation fluctuations, synchrotron polarization gradients (SPGs) and synchrotron polarization derivative gradients (SPDGs) can reveal more detailed information on the turbulent magnetic field. In particular, the latter can sample the spatial regions close to the observer with the sampling depth controlled by the radiation wavelength (see **Figure 1**), which provides a new approach to map the 3D distribution of Galactic magnetic fields.

Specifically, the de-correlation of the Faraday rotation measure is introduced as (LP16; Zhang et al., 2020)

$$\lambda^2\Phi = 0.81\lambda^2\int_0^{L_{\text{eff}}} dz n_e B_\parallel = 2\pi, \tag{65}$$

where L_{eff} is an effective spatial depth of the Faraday rotation sampling. We can thus write the ratio of the depth sampled by the Faraday rotation to the emitting region size as

$$\frac{L_{\text{eff}}}{L} \approx \frac{2\pi}{\lambda^2 L}\frac{1}{\phi}, \tag{66}$$

with $\phi = \max(\sqrt{2}\sigma_\phi, \bar{\phi})$. Here, σ_ϕ denotes the root mean square and $\bar{\phi}$ Faraday rotation density. According to **Eq 66**, the strong and weak depolarizations can be characterized by $L_{\text{eff}}/L < 1$ and $L_{\text{eff}}/L > 1$, respectively. In the case of the strong depolarization, the entire space is divided into two different parts as shown in **Figure 1**, from which we can know that only the part of $z < L_{\text{eff}}$ experiences the depolarization while the part of $z > L_{\text{eff}}$ cannot contribute to the polarization correlation. When observing
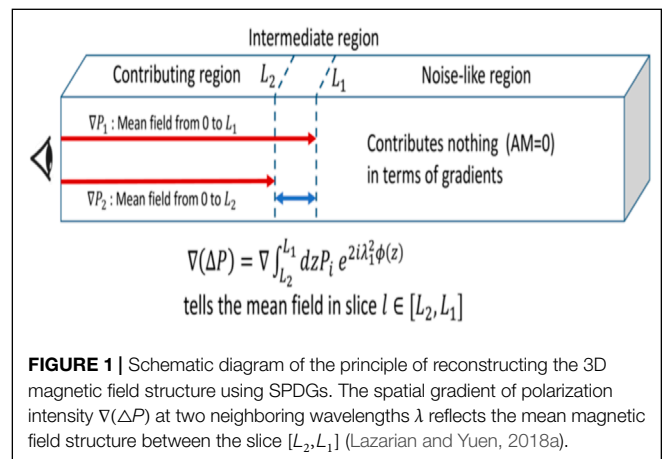
FIGURE 1 | Schematic diagram of the principle of reconstructing the 3D magnetic field structure using SPDGs. The spatial gradient of polarization intensity $\nabla(\triangle P)$ at two neighboring wavelengths λ reflects the mean magnetic field structure between the slice $[L_2, L_1]$ (Lazarian and Yuen, 2018a).

that the frequency interval $\triangle v = c/\lambda^2 \triangle \lambda$ is small enough, the difference of $\mathbf{P}(\lambda_1)$ and $\mathbf{P}(\lambda_2)$ in the range of $[L_2, L_1]$ is written as

$$\triangle \mathbf{P} \approx \int_{L_2}^{L_1} dz \mathbf{P}_i(\mathbf{X}, z) e^{2i\lambda^2 \Phi(\mathbf{X}, z)}, \quad (67)$$

from which the expression of the SPDGs is given by

$$\nabla \frac{d|\mathbf{P}|}{d\lambda^2} \sim \lambda^{-2} \nabla |\mathbf{P}(\lambda_1) - \mathbf{P}(\lambda_2)|. \quad (68)$$

From another perspective, namely, based on the spatial gradient analysis of Stokes parameters Q and U on the complex plane, Gaensler et al. (2011) proposed the synchrotron polarization gradients to constrain the sonic Mach number in warm or ionized ISM. After a simple mathematical derivation, the spatial gradient of polarization intensity can be expressed as

$$|\nabla P| = \sqrt{\left(\frac{\partial Q}{\partial x}\right)^2 + \left(\frac{\partial U}{\partial x}\right)^2 + \left(\frac{\partial Q}{\partial y}\right)^2 + \left(\frac{\partial U}{\partial y}\right)^2}. \quad (69)$$

Subsequently, considering rotational and translational invariance of coordinates, various diagnostic quantities were developed by Herron et al. (2018).

5 APPLICATIONS OF STATISTICAL TECHNIQUES

5.1 Measurement of Scaling Slope

LP12 predicted that the power spectrum, correlation, and structure functions of synchrotron radiation fluctuations, termed two-point statistics, can recover the scaling slope of turbulent magnetic fields. Numerical simulations show that the correlation function does not work in revealing scaling slopes, but it can be used to explore the correlation scale and the effect of the electron spectral index on turbulence (Herron et al., 2016; Lee et al., 2016; Zhang et al., 2016). The main reason that we think is that LP16 performed theoretical studies under the condition of the power-law correlation model, from which they predicted the possibility of obtaining the scaling slope for the corresponding model. The correlation function itself, however, has a divergent behavior for numerical simulation or observational data, because Stokes parameters Q and U contain the information of negative values arising from the change in the direction of the turbulent magnetic field.

Numerical results demonstrated that the scaling slope of the underlying MHD turbulence can be recovered approximately by the two-point structure function of synchrotron radiation fluctuations (Lee et al., 2016). From the perspective of numerical simulations, the direct calculation of the spatial structure function is more time-consuming, compared with the correlation function or power spectrum. Alternatively, one can first get the statistics of the correlation function, provided that it maintains convergence, and then calculate the structure function using the relation of $SF(\mathbf{R}) = 2[CF(0) - CF(\mathbf{R})]$. In general, the two-point structure functions are unable to correctly reproduce the scaling of a spectrum with a slope ~ -3 or steeper (sometimes

problems may arise already at slopes slightly shallower than -3, if the underlying spectrum is not a perfect power-law). For instance, Lee et al. (2016) measured the scaling slope of 5/3 with the change in a numerical resolution. It was pointed out that the scaling slope of the two-point structure function, calculated directly from 2D synthetic data, was still less than 5/3 expected for the Kolmogorov spectrum, even with a 8192^2 resolution. Thus, using a two-point structure function to extract the scaling slope of turbulence requires more precise statistics with a higher numerical resolution. Alternatively, the multi-point structure functions are recommended to achieve better convergence of the results (see Cho and Lazarian, 2009; Cho, 2019).

Obtaining the scaling slope through the power spectrum of synchrotron fluctuations should be one of the most efficient ways, as the calculation of the power spectrum invokes the fast Fourier transform in the wavenumber space to effectively accelerate the process. Adopting both synthetic and MHD turbulence simulation data, Lee et al. (2016) obtained the power spectrum and its derivative with respect to the wavelength of synchrotron polarization arising from synchrotron polarization radiation together with Faraday rotation fluctuations. This study succeeded in obtaining the scaling slope and demonstrated that simulations are in agreement with the theoretical prediction in LP16. In addition, using simulated interferometric observations on how to recover the scaling slope was also attempted. Notice that the study mentioned previously is based on the spatially coincident synchrotron emission and Faraday rotation regions. Furthermore, considering spatially separated and compounded synchrotron radiation and Faraday rotation fluctuations, Zhang et al. (2018) studied how to extract the scaling slope of synchrotron polarization intensities. In the short wavelength range, the power spectra revealed fluctuation statistics of the perpendicular component of turbulent magnetic fields, and the spectra reflected the fluctuation of the Faraday rotation in the long-wavelength range. As shown in **Figure 2**, the effects of telescope angular resolution and noise structure do not hinder the use of power spectrum methods to obtain scaling slopes of MHD turbulence in the large-scale inertial range.

Motivated by one-point statistics in LP16 (termed PFA), which is characterized by the variance of polarized emission as a function of the squared wavelength along a single line of sight, Zhang et al. (2016) studied how to extract the scaling slope of underlying MHD turbulence. To depict the level of turbulence, they defined a ratio η of the standard deviation of the line of sight turbulent magnetic field to the line of sight mean magnetic field. As shown in **Figure 3**, a large ratio ($\eta \gg 1$) characterizing a turbulent field dominated regime reflects the polarization variance $\langle\langle P^2 \rangle\rangle \propto \lambda^{-2}$, and a small ratio ($\eta \lesssim 0.2$) characterizing a mean field-dominated regime reveals the polarization variance $\langle\langle P^2 \rangle\rangle \propto \lambda^{-2-2m} = \lambda^{-10/3}$ with $m = 2/3$ for the Kolmogorov scaling. As a result, the turbulent spectral index was successfully recovered by the polarization variance in the case of the mean field-dominated regime, i.e., a small η. At the same time, it was pointed out that the change in cosmic ray electron spectral indices cannot affect the scaling slope measurement of magnetic turbulence. This provides a new

FIGURE 2 | The influences of telescope angular resolution (left panel) and Gaussian noise (right panel) on the power spectrum calculated at the wavelength λ =2.4 in code units. The symbol $\Delta\sigma$ indicating standard deviation of Gaussian noise accounts for a fraction of the mean synchrotron polarization intensity. The symbol θ_{FWHM} denoting an effective Gaussian beam is used to convolve 2D maps of Stokes parameters. The original (ideal) slope without considering the resolution and noise is shown in the solid line (Zhang et al., 2018).

method for recovering the scaling index of MHD turbulence and agrees with the theoretical prediction of LP16. Interestingly, this technique has been successfully applied to explain the depolarization in the optical wavebands from active galactic nuclei (Guo et al., 2017).

5.2 Measurement of Anisotropy

As described in **Section 2**, the prediction of the anisotropy (eddy's elongation along the local magnetic field direction) in turbulent cascade is an important contribution of GS95. It is

FIGURE 3 | The transition of polarization variance from the stochastic Faraday rotation fluctuation dominant regime for $\eta = \infty$, to the uniform fluctuation dominant one for η =0.080 in 3D synthetic simulation with a resolution of 4096^3. The underlying MHD turbulence corresponds to the Kolmogorov spectrum of the index 11/3 (Zhang et al., 2016).

challenging to test the local anisotropy of MHD turbulence from an observational point of view because the observational signal is inevitably involved in the integration along the line of sight in the observer's frame of reference. Note that integrated synchrotron fluctuations along the line of sight were predicted by LP12 to be anisotropic, with the eddy's major axis aligned with the direction of the mean magnetic field instead of the local field within the MHD turbulence volume.

The spatial second-order structure function of radiation fluctuations is a very direct way to reveal the existence of anisotropy in MHD turbulence, although the anisotropy here does not directly correspond to the local anisotropy favored by the modern MHD turbulence theory. By visualizing a contour map for 2D structure function of observations, one can easily see the anisotropic distribution, from which the major axis direction of the elongated structure will qualitatively characterize the mean magnetic field orientation (see **Figure 1** in Wang R. Y et al. (2020) for an example). Considering the ratio of two measurement directions perpendicular to each other from observed polarization intensities, called an anisotropic coefficient, we can quantitatively determine the degree of the anisotropy of the MHD turbulence in the global frame of the reference; refer to the work of Lee et al. (2019) and Wang R. Y et al. (2020) for more details.

A new more precise method to measure the anisotropy is termed as the quadrupole ratio described in **Section 4**. This method was proposed in LP12 that derives many analytical formulae including the predictions from the Alfvén, slow, and fast modes in the high or low β plasma regime. A numerical test of theoretical predictions on the quadrupole ratio was attempted by Herron et al. (2016) based on MHD turbulence simulation. We have to point out that their testing used a simplified version rather than a general formula. In particular, they adopted the compressible MHD turbulence data to study the isotropic version of formulae, which fails to provide proof of the usability of the analytical formula. Considering the angle change in between the
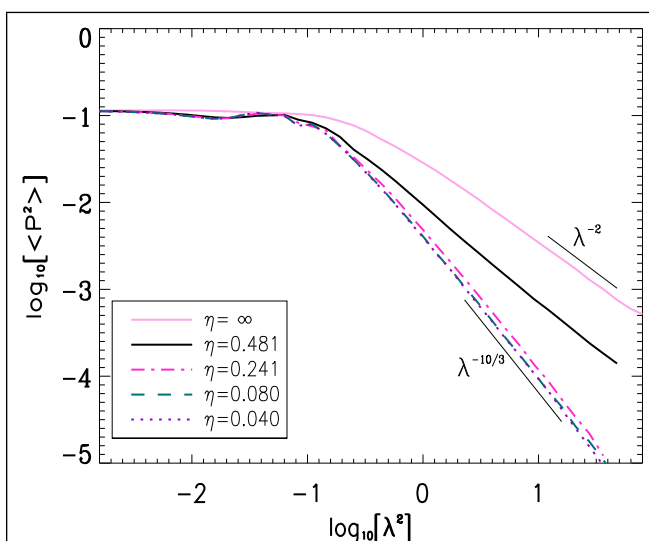
mean magnetic field direction and the line of sight, recently tested the theoretical prediction of LP12 in detail and confirmed the correctness of the analytical formulae, providing convenience to study the anisotropy of MHD turbulence by using the analytical expressions.

How the anisotropic structure changes with observation frequency were studied in Lee et al. (2019) by the quadrupole ratio. Their studies showed that in the high-frequency range, the observed polarization exhibits the averaged structures of both foreground and background regions, while in the low-frequency range, the large-scale structures are wiped out by a strong Faraday depolarization and the small-scale anisotropy reflects the magnetic field structure from the foreground region.

By decomposing the compressible MHD turbulence into three plasma modes, i.e., Alfvén, slow, and fast modes, Wang R. Y et al. (2020) demonstrated that the quadrupole ratio statistics of the polarization intensity from the Alfvén and slow modes present a significant anisotropy, while the fast mode statistics show isotropic structures (see **Figure 4**). Those findings are in agreement with the earlier direct numerical simulations provided in CL02. As a result, the quadrupole ratio method can be applied to the measurement of the anisotropy of MHD turbulence in various astrophysical environments.

5.3 Measurement of Magnetic Field Orientations

The traditional method of measuring the magnetic field direction is called the synchrotron polarization vector, which is based on the fact that the observed polarization vectors are perpendicular to the magnetic field directions within the emitting source. Note that the limitation of this method cannot be applied to observations with Faraday rotation.

Using synchrotron intensity gradients (SIGs) together with both MHD turbulence simulation and PLANCK archive data,

Lazarian et al. (2017) demonstrated the practical applicability of the gradient technique described in **Section 4**, comparing the measured directions of magnetic fields arising from the gradient technique with that of the traditional polarization vector method. Furthermore, SIGs were advanced in Lazarian and Yuen (2018a) to SPGs and SPDGs. Subsequently, to explore the magnetic field measurement capabilities of synchrotron gradient techniques, SPGs and SPDGs were generalized and applied to a variety of possible astrophysical environments in a series of studies including different turbulence regimes, the gradient of various diagnostic quantities, realistic observations of Galactic diffuse media, as well as spatially separated synchrotron radiation and Faraday depolarization regions.

5.3.1 Gradient Measurement in Various Turbulence Regimes

Based on synthetic observations from MHD turbulence simulations, Zhang et al. (2019a) extended both SPGs and SPDGs to super-Alfvénic regimes and studied how to trace the directions of turbulent magnetic fields. Focusing on multi-frequency measurements in the presence of strong Faraday rotation, they provided the procedures of how to recover the projected mean magnetic fields on the plane of the sky and the local magnetic fields within a tomographic slice. The results demonstrated that in the low-frequency strong Faraday rotation regime, the SPGs had a significant advantage over the traditional polarization vector method in tracing projected mean magnetic fields and the SPDGs were applicable to tracing the local magnetic field directions in the local frame of reference of MHD turbulence. At the same time, their parameter research provided a testing ground for the application of the new techniques to a large number of data cubes, such as those from LOFAR and SKA.

FIGURE 4 | Quadrupole ratio of synchrotron polarization intensities for Alfvén, slow, and fast modes as a function of radial separation of maps in the sub-Alfvénic regime (Wang R. Y et al., 2020).
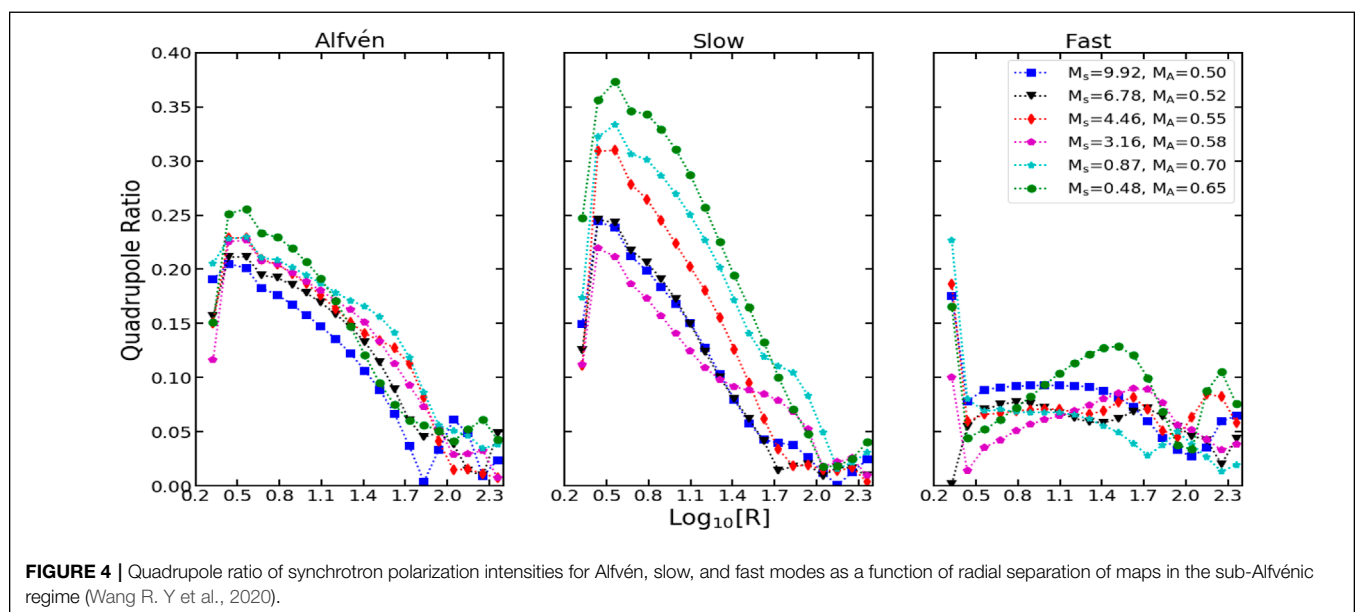
5.3.2 Gradient Measurement of Various Diagnostic Quantities

The various diagnostic quantities, including the polarization directional curvature, polarization wavelength derivative, and polarization wavelength curvature, are derived in Herron et al. (2018) considering the translational and rotational invariance of the observed quantities. It is noticed that the authors were not aware of the relation between the magnetic field direction and the gradients of synchrotron radiation gradients, and did not explore whether the new diagnostics they introduced could trace magnetic field in observations.

The spatial gradients of various diagnostics provided in the work of Herron et al. (2018) have been proposed to trace the directions of the mean magnetic field by Zhang et al. (2019b), who found that the gradients of various diagnostics can effectively determine the direction of the projected magnetic fields on the plane of the sky. One of these techniques, namely the maximum of the radial component of the polarization directional derivative, is the best robust method for tracing the mean magnetic field directions in the Galactic ISM.

The synergy of various diagnostic gradients is complementary in tracing the actual direction of interstellar magnetic fields, especially in the low-frequency Faraday rotation regime where the traditional polarization vector method cannot work. Applying the synergies of synchrotron diagnostic gradients to the archive data from the Canadian Galactic Plane Survey (*Taylor et al., 2003*), *Zhang et al. (2019b)* showed that various diagnostic techniques make consistent predictions for the Galactic mean magnetic field directions.

5.3.3 Gradient Measurement of Spatially Separated Regions

When confronted with realistic observations, the synchrotron polarization radiation obtained by the observers could originate from complex turbulence regions rather than a single spatially coincident radiation and a Faraday rotation region. Can the synchrotron polarization gradient still measure the direction of the magnetic field for more complex astrophysical settings?

The measurement capabilities of the SPGs were studied in Wang et al. (2021) by constructing spatially separated models, focusing on exploring how the Faraday rotation density in the foreground region affects the measurement of the projected magnetic field. Their numerical results showed that the use of the SPG technique for a complex astrophysical environment could successfully trace the projected mean magnetic field direction within the emitting source region independent of radiation frequency.

5.3.4 Measurement of the Local Magnetic Field Direction

Thanks to the inevitable accumulation of the observed signal along the line of sight, i.e., less locality, it is extremely challenging to measure the local magnetic field in MHD turbulence. However, the measurement of the local magnetic field will be the direct evidence to verify the modern MHD turbulence anisotropy theory since this theory is based on the local magnetic field reference system (see **Section 2.3.1**). At the same time, the acquisition of the local magnetic field information is a pre-requisite for reconstructing the Galactic 3D magnetic field as well.

Using gradient statistics of the synchrotron polarization derivative with respect to the squared wavelength $dP/d\lambda^2$, the measurement of the local magnetic field direction has been implemented in Zhang et al. (2020) based on data cubes obtained with MHD turbulence simulations. They demonstrated that in the low-frequency strong Faraday rotation regime, the statistic analysis of the spatial gradient of $dP/d\lambda^2$ can indeed reveal the local magnetic field direction and the local anisotropy of the underlying MHD turbulence which increases with increasing radiation frequency.

As illustrated in **Figure 1**, this technique can successfully extract the local information of MHD turbulence in the tomography space along the line of sight by using multi-frequency observations at adjacent frequencies. Unlike the traditional Faraday rotation synthesis (e.g., Burn, 1966), the polarization gradient techniques are not affected by the Faraday rotation and can improve the 3D model of the Galactic magnetic field effectively.

5.4 Measurement of Magnetization Strength

Several statistical methods, such as Genus, Tsallis, skewness, and kurtosis statistics, are sensitive to the magnetization level M_A of MHD turbulence (e.g., Burkhart et al., 2012; Herron et al., 2016). In addition, the correlation function (e.g., Lazarian et al., 2002; Burkhart et al., 2014; Esquivel et al., 2015) and structure function (Hu et al., 2021; Xu and Hu, 2021) analysis are also suggested as alternative techniques of measuring M_A. At present, these studies are based on the velocity information analysis from MHD turbulence simulations. Similarly, the adoption of synchrotron fluctuations should be on the agenda.

In analogy with velocity gradient techniques, Lazarian et al. (2018b) first discussed that synchrotron gradient techniques should be able to measure the magnetization level. The feasibility of the two methods was explored in Carmo et al. (2020) to obtain the level of magnetization from synchrotron polarization fluctuation, namely the top-base and the circular standard deviation. They claimed that the signal-to-noise ratio was more severe for the top-base method, but still reliable with the standard deviation method. In short, the finding on the power-law relation between M_A and synchrotron gradient statistics is important for determining M_A from the current or future available data cubes.

6 DISCUSSION

The progress in understanding the role of magnetic fields for processes in a specific astrophysical environment depends on our ability to obtain their properties from MHD turbulence. Unfortunately, it is notoriously difficult for studying the properties of magnetic fields. In practice, almost every technique presents its limits. For example, the difficulty with dust polarization measurement lies in the inability to measure the

magnetic field strength along the line of sight and insufficient dust grain alignment efficiencies at low Galactic latitudes, preventing observers from deriving the information of magnetic fields in the ISM. For another example, the difficulty with Zeeman splitting measurement is that it can only measure the line of sight component strength of the magnetic field, access the high magnitude end of the interstellar magnetic fields in a mildly turbulent environment, and provide limited morphology information (Crutcher, 2009). Last but not least, a serious limitation of the well-known Faraday tomography is that the line of sight component of the magnetic field in turbulence is expected to change its sign, resulting in the Faraday depth to become ambiguous (see Ho et al., 2019 for a comparison of measure performance between Faraday tomography and SPGs; refer also to Akahori et al., 2018 for the recent review on other more methods and applications in specific astrophysics).

The further development of related new techniques can potentially extract other properties of MHD turbulence. In the framework of synchrotron fluctuations, many topics deserve to be further studied. As an example, visualization of the structure or correlation functions of synchrotron diagnostics can present an anisotropic feature, by which one could trace the mean magnetic field orientations and measure magnetization strength. It should be encouraged to explore the feasibility of this technique for measuring magnetic fields, the fundamental spirit of which is similar to the correlation function anisotropy technique on velocity information (Lazarian et al., 2002; Esquivel and Lazarian, 2005; Hu et al., 2021; Xu and Hu, 2021). We would like to emphasize that the synchrotron dispersion techniques discussed currently are also complementary to other techniques of magnetic field studies, such as velocity channel analysis, velocity coordinate analysis, and velocity gradient techniques. The synergistic use of multiple techniques is necessary because one will be able to improve the reliability of magnetic field measurements by fully utilizing the advantages of each technique.

None of the relevant articles covered in this review consider synchrotron self-absorption effects (see **Section 3** for self-absorption processes). However, when the brightness temperature of synchrotron radiation approaches the 'thermal' temperature of emitting relativistic electrons, the synchrotron self-absorption effect is expected to be important in the case of low frequencies. In the framework of new techniques developed, we expect that the effects of self-absorption can provide yet another method of testing the 3D structure of the magnetic field. Indeed, only the regions closer to the observer and less affected by self-absorption are expected to be probed under strong self-absorption. This effect is similar to the effect of the dust self-absorption in spectral line statistics that was explored analytically in Kandel et al. (2017b) and numerically in Yang et al. (2021).

In the recent studies related to synchrotron radiation techniques, one simply assumes a homogeneous, isotropic, non-thermal relativistic electron distribution with a power-law energy spectrum. In fact, the specific properties of the relativistic electrons would depend on the cascade process of MHD turbulence, that is, it is also necessary to solve the so-called turbulent heating problem between MHD scales and electron plasma scales. Since part of the initial cascading turbulent energy

will be removed by the ion heating/energizing at ion scales before it reaches the electron scales, only a fraction of the energy cascading from the large MHD scales will end up in heating/energizing the electrons which will determine a specific spectral energy distribution $N(E)$ to produce the observed synchrotron radiation. What is this fraction is currently a big open question and answering it would require understanding on what happens at turbulent fluctuations during the transition from MHD scales to kinetic scales, as well as the role of various collisionless processes leading to particle heating that could be at work within different plasma regimes (e.g., Quataert, 1998; Schekochihin et al., 2009; Chandran et al., 2010; Cranmer, 2014; Arzamasskiy et al., 2019; Cerri et al., 2019; Zhdankin et al., 2019; Vasquez et al., 2020; Cerri et al., 2021). As a result, different anisotropy models (i.e., different turbulence theories at MHD scales; see **Section 2.5**) would determine different properties of fluctuations at kinetic scales which are essential to determine the differential heating of ions and electrons.

Compared to the Faraday rotation synthesis to obtain the 3D magnetic fields in the galaxies (e.g., Burn, 1966; Beck, 2015), where the Faraday depth is changing its sign along the line of sight, making the determination of the magnetic field component $B_\parallel$ ambiguous (see Ferriere, 2016), the advantage of the polarization gradient technique is that it is not affected by Faraday rotation and will effectively improve the measurement of our current Galactic 3D magnetic field model. The correct understanding of this model, as a fundamental ingredient, is indeed very important, e.g., for modeling the anisotropic cosmic ray propagation in the Galaxy (e.g., Cerri et al., 2017; Reichherzer et al., 2022) which can explain some anomalies inferred from gamma-ray emission (Acero et al., 2016; Yang et al., 2016), and is critical to obtain a realistic Galactic evolution (e.g., Beck, 2015).

Furthermore, an accurate understanding of Galactic magnetic fields is indispensable for searching the B modes of the Cosmic Microwave Background (CMB, Zucca et al., 2017), which is essential for understanding the evolution of the early Universe. The CMB B mode studies require more accurate removal of the Galactic foreground contamination, which is achievable provided that the detailed information of Galactic magnetic fields can be obtained (e.g., Cho and Lazarian, 2010). Therefore, it is promising that using the new synchrotron gradients performs foreground removal for studying the CMB B modes on the plane of the sky. We expect that there are different properties between the Galactic foreground SPGs and cosmological perturbation one, that is, the direction traced by the former is perpendicular to the foreground polarization, while the latter does not follow this relation. In addition, the CMB E and B mode ratio has been demonstrated to be sensitive to the fraction of the fast modes in MHD turbulence and the magnetization strength (Kandel et al., 2017a). Furthermore, one can obtain the local properties of the CMB E and B modes using the SPDGs, which provide an alternative way of studying the distribution of compressible MHD turbulence modes over the sky and of determining the magnetization level of the Galactic ISM.

Most of the work that has been carried out is based on numerical simulations, which, on the one hand, helps

to test the feasibility of the technique and, on the other hand, provides the test grounds for studying magnetic fields using a large number of data cubes from the LOFAR and SKA. Hence, the next step is necessary to advance the application of the technique using observational data to test the performance of the technique in a specific astrophysical setting.

AUTHOR CONTRIBUTIONS

All authors listed have made a substantial contribution to the work and approved it for publication.

FUNDING

ACKNOWLEDGMENTS

REFERENCES

Acero, F., Ackermann, M., Ajello, M., Albert, A., Baldini, L., Ballet, J., et al. (2016). Development of the Model of Galactic Interstellar Emission for Standard Point-source Analysis of Fermi Large Area Telescope Data. *ApJS* 223, 26. doi:10.3847/0067-0049/223/2/26

Akahori, T., Nakanishi, H., Sofue, Y., Fujita, Y., Ichiki, K., Ideguchi, S., et al. (2018). Cosmic Magnetism in Centimeter- and Meter-Wavelength Radio Astronomy. *PASJ* 70, R2. doi:10.1093/pasj/psx123

Armstrong, J. W., Rickett, B. J., and Spangler, S. R. (1995). Electron Density Power Spectrum in the Local Interstellar Medium. *ApJ* 443, 209–221. doi:10.1086/175515

Arzamasskiy, L., Kunz, M. W., Chandran, B. D. G., and Quataert, E. (2019). Hybrid-kinetic Simulations of Ion Heating in Alfvénic Turbulence. *ApJ* 879, 53. doi:10.3847/1538-4357/ab20cc

Beck, R. (2015). Magnetic fields in Spiral Galaxies. *Astron. Astrophys Rev.* 24, 4. doi:10.1007/s00159-015-0084-4

Beresnyak, A. (2013). Erratum: Basic Properties of Magnetohydrodynamic Turbulence in the Inertial Range. *MNRAS* 432, 3546. doi:10.1093/mnras/stt685

Beresnyak, A., and Lazarian, A. (2010). Scaling Laws and Diffuse Locality of Balanced and Imbalanced Magnetohydrodynamic Turbulence. *ApJ* 722, L110–L113. doi:10.1088/2041-8205/722/1/L110

Beresnyak, A., and Lazarian, A. (2019). *Turbulence in Magnetohydrodynamics*. Berlin: Springer.

Beresnyak, A. (2019). MHD Turbulence. *Living Rev. Comput. Astrophys* 5, 2. doi:10.1007/s41115-019-0005-8

Beresnyak, A. (2014). Spectra of Strong Magnetohydrodynamic Turbulence from High-Resolution Simulations. *ApJ* 784, L20. doi:10.1088/2041-8205/784/2/l20

Beresnyak, A. (2017). Three-dimensional Spontaneous Magnetic Reconnection. *ApJ* 834, 47. doi:10.3847/1538-4357/834/1/47

Biskamp, D. (2003). *Magnetohydrodynamic Turbulence*. Cambridge: Cambridge University Press.

Boldyrev, S., Nordlund, A., and Padoan, P. (2002b). Scaling Relations of Supersonic Turbulence in Star-forming Molecular Clouds. *ApJ* 573, 678–684. doi:10.1086/340758

Boldyrev, S., Nordlund, Å., and Padoan, P. (2002a). Supersonic Turbulence and Structure of Interstellar Molecular Clouds. *Phys. Rev. Lett.* 89, 031102. doi:10.1103/PhysRevLett.89.031102

Boldyrev, S. (2005). On the Spectrum of Magnetohydrodynamic Turbulence. *ApJ* 626, L37–L40. doi:10.1086/431649

Boldyrev, S. (2006). Spectrum of Magnetohydrodynamic Turbulence. *Phys. Rev. Lett.* 96, 115002. doi:10.1103/physrevlett.96.115002

Brandenburg, A., and Subramanian, K. (2005). Astrophysical Magnetic fields and Nonlinear Dynamo Theory. *Phys. Rep.* 417, 1–209. doi:10.1016/j.physrep.2005.06.005

Bruno, R., and Carbone, V. (2013). The Solar Wind as a Turbulence Laboratory. *Living Rev. Solar Phys.* 10, 2. doi:10.12942/lrsp-2013-2

Bu, D.-F., Wu, M.-C., and Yuan, Y.-F. (2016). Effects of Anisotropic thermal Conduction on Wind Properties in Hot Accretion Flow. *Mon. Not. R. Astron. Soc.* 459, 746–753. doi:10.1093/mnras/stw723

Burkhart, B., Lazarian, A., and Gaensler, B. M. (2012). Properties of Interstellar Turbulence from Gradients of Linear Polarization Maps. *ApJ* 749, 145. doi:10.1088/0004-637x/749/2/145

Burkhart, B., Lazarian, A., Leão, I. C., de Medeiros, J. R., and Esquivel, A. (2014). Measuring the Alfvénic Nature of the Interstellar Medium: Velocity Anisotropy Revisited. *ApJ* 790, 130. doi:10.1088/0004-637X/790/2/130

Burn, B. J. (1966). On the Depolarization of Discrete Radio Sources by Faraday Dispersion. *Monthly Notices R. Astronomical Soc.* 133, 67–83. doi:10.1093/mnras/133.1.67

Carmo, L., González-Casanova, D. F., Falceta-Gonçalves, D., Lazarian, A., Jablonski, F., Zhang, J.-F., et al. (2020). Synchrotron Intensity and Polarization Gradients: Tools to Obtain the Magnetization Level in a Turbulent Medium. *ApJ* 905, 130. doi:10.3847/1538-4357/abc331

Carroll, J., Frank, A., Blackman, E. G., Cunnningham, A. J., and Quillen, A. C. (2009). "Outflow-Driven Turbulence in Molecular Clouds. *ApJ* 695, 1376–1381. doi:10.1088/0004-637X/695/2/1376

Cerri, S. S., Arzamasskiy, L., and Kunz, M. W. (2021). On Stochastic Heating and its Phase-Space Signatures in Low-Beta Kinetic Turbulence. *ApJ* 916, 120. doi:10.3847/1538-4357/abfbde

Cerri, S. S., and Califano, F. (2017). Reconnection and Small-Scale fields in 2d-3v Hybrid-Kinetic Driven Turbulence Simulations. *New J. Phys.* 19, 025007. doi:10.1088/1367-2630/aa5c4a

Cerri, S. S., Gaggero, D., Vittino, A., Evoli, C., and Grasso, D. (2017). A Signature of Anisotropic Cosmic-ray Transport in the Gamma-ray Sky. *J. Cosmol. Astropart. Phys.* 2017, 019. doi:10.1088/1475-7516/2017/10/019

Cerri, S. S., Grošelj, D., and Franci, L. (2019). Kinetic Plasma Turbulence: Recent Insights and Open Questions from 3D3V Simulations. *Front. Astron. Space Sci.* 6, 64. doi:10.3389/fspas.2019.00064

Chamandy, L., and Shukurov, A. (2020). Parameters of the Supernova-Driven Interstellar Turbulence. *Galaxies* 8, 56. doi:10.3390/galaxies8030056

Chandran, B. D. G. (2005). AGN-driven Convection in Galaxy-Cluster Plasmas. *ApJ* 632, 809–820. doi:10.1086/432596

Chandran, B. D. G., Li, B., Rogers, B. N., Quataert, E., and Germaschewski, K. (2010). Perpendicular Ion Heating by Low-Frequency Alfvén-Wave Turbulence in the Solar Wind. *ApJ* 720, 503–515. doi:10.1088/0004-637x/720/1/503

Chandran, B. D. G., Schekochihin, A. A., and Mallet, A. (2015). Intermittency and Alignment in Strong RMHD Turbulence. *ApJ* 807, 39. doi:10.1088/0004-637X/807/1/39

Chen, C. H. K., Mallet, A., Yousef, T. A., Schekochihin, A. A., and Horbury, T. S. (2011). Anisotropy of Alfvénic Turbulence in the Solar Wind and Numerical Simulations. *MNRAS* 415, 3219–3226. doi:10.1111/j.1365-2966.2011.18933.x

Chepurnov, A., and Lazarian, A. (2010). Extending the Big Power Law in the Sky with Turbulence Spectra from Wisconsin Hα Mapper Data. *ApJ* 710, 853–858. doi:10.1088/0004-637X/710/1/853

Cho, J. (2019). A Technique for Removing Large-Scale Variations in Regularly and Irregularly Spaced Data. *ApJ* 874, 75. doi:10.3847/1538-4357/ab06f3

Cho, J., and Lazarian, A. (2003). Compressible Magnetohydrodynamic Turbulence: Mode Coupling, Scaling Relations, Anisotropy, Viscosity-Damped Regime and Astrophysical Implications. *MNRAS* 345, 325–339. doi:10.1046/j.1365-8711.2003.06941.x

Cho, J., and Lazarian, A. (2002). Compressible Sub-alfvénic MHD Turbulence in Low-βPlasmas. *Phys. Rev. Lett.* 88, 245001. doi:10.1103/PhysRevLett.88.245001

Cho, J., and Lazarian, A. (2010). Galactic Foregrounds: Spatial Fluctuations and a Procedure for Removal. *ApJ* 720, 1181–1201. doi:10.1088/0004-637X/720/2/1181

Cho, J., and Lazarian, A. (2009). Simulations of Electron Magnetohydrodynamic Turbulence. *ApJ* 701, 236–252. doi:10.1088/0004-637X/701/1/236

Cho, J., and Vishniac, E. T. (2000). The Anisotropy of Magnetohydrodynamic Alfvenic Turbulence. *ApJ* 539, 273–282. doi:10.1086/309213

Cranmer, S. R. (2014). Ensemble Simulations of Proton Heating in the Solar Wind via Turbulence and Ion Cyclotron Resonance. *ApJS* 213, 16. doi:10.1088/0067-0049/213/1/16

Crusius, A., and Schlickeiser, R. (1986). Synchrotron Radiation in Random Magnetic fields. *A&A* 164, L16–L18.

Crutcher, R. M. (2012). Magnetic Fields in Molecular Clouds. *Annu. Rev. Astron. Astrophys.* 50, 29–63. doi:10.1146/annurev-astro-081811-125514

Crutcher, R. M. (2009). OH and CN Zeeman Observations of Magnetic Fields in Molecular Clouds. *Revista Mexicana de Astronomia y Astrofisica* 36, 107–112. (Instituto de Astronomía). Available at: https://ui.adsabs.harvard.edu/abs/2009RMxAC.36.107C/abstract.

Dib, S., Bell, E., and Burkert, A. (2006). The Supernova Rate-Velocity Dispersion Relation in the Interstellar Medium. *ApJ* 638, 797–810. doi:10.1086/498857

Dib, S., Braine, J., Gopinathan, M., Lara-López, M. A., Kravtsov, V. V., Soam, A., et al. (2021). The Structure and Characteristic Scales of the H I Gas in Galactic Disks. *A&A* 655, A101. doi:10.1051/0004-6361/202141803

Dib, S., Hennebelle, P., Pineda, J. E., Csengeri, T., Bontemps, S., Audit, E., et al. (2010). The Angular Momentum of Magnetized Molecular Cloud Cores: A Two-Dimensional-Three-Dimensional Comparison. *ApJ* 723, 425–439. doi:10.1088/0004-637X/723/1/425

Dobrowolny, M., Mangeney, A., and Veltri, P. (1980). Properties of Magnetohydrodynamic Turbulence in the Solar Wind. *A&A* 83, 26–32. doi:10.1007/978-94-009-9100-2_20

Dong, C., Wang, L., Huang, Y.-M., Comisso, L., and Bhattacharjee, A. (2018). Role of the Plasmoid Instability in Magnetohydrodynamic Turbulence. *Phys. Rev. Lett.* 121, 165101. doi:10.1103/PhysRevLett.121.165101

Esquivel, A., Lazarian, A., and Pogosyan, D. (2015). Studying the Interstellar Magnetic Field from Anisotropies in Velocity Channels. *ApJ* 814, 77. doi:10.1088/0004-637x/814/1/77

Esquivel, A., and Lazarian, A. (2005). Velocity Centroids as Tracers of the Turbulent Velocity Statistics. *ApJ* 631, 320–350. doi:10.1086/432458

Falgarone, E., and Passot, T. (2003). *Turbulence and Magnetic Fields in Astrophysics.* Berlin: Springer.

Federrath, C. (2016). Magnetic Field Amplification in Turbulent Astrophysical Plasmas. *J. Plasma Phys.* 82, 535820601. doi:10.1017/S0022377816001069

Ferrière, K. (2016). Faraday Tomography: a New, Three-Dimensional Probe of the Interstellar Magnetic Field. *J. Phys. Conf. Ser.* 767, 012006. doi:10.1088/1742-6596/767/1/012006

Fornieri, O., Gaggero, D., Cerri, S. S., De La Torre Luque, P., and Gabici, S. (2021). The Theory of Cosmic ray Scattering on Pre-existing MHD Modes Meets Data. *MNRAS* 502, 5821–5838. doi:10.1093/mnras/stab355

Franci, L., Cerri, S. S., Califano, F., Landi, S., Papini, E., Verdini, A., et al. (2017). Magnetic Reconnection as a Driver for a Sub-ion-scale Cascade in Plasma Turbulence. *ApJ* 850, L16. doi:10.3847/2041-8213/aa93fb

Fromang, S. (2013). MRI-driven Angular Momentum Transport in Protoplanetary Disks. *EAS Publ. Ser.* 62, 95–142. Editors P. Hennebelle, and C. Charbonnel (EAS Publications Series). doi:10.1051/eas/1362004

Gaches, B. A. L., Walch, S., and Lazarian, A. (2021). Cosmic-Ray Acceleration from Turbulence in Molecular Clouds. *ApJL* 917, L39. doi:10.3847/2041-8213/ac1b2f

Gaensler, B. M., Haverkorn, M., Burkhart, B., Newton–McGee, K. J., Ekers, R. D., Lazarian, A., et al. (2011). Low-Mach-number Turbulence in Interstellar Gas Revealed by Radio Polarization Gradients. *Nature* 478, 214–217. doi:10.1038/nature10446

Galtier, S., Nazarenko, S. V., Newell, A. C., and Pouquet, A. (2000). A Weak Turbulence Theory for Incompressible Magnetohydrodynamics. *J. Plasma Phys.* 63, 447–488. doi:10.1017/S0022377899008284

Gardiner, T. A., and Stone, J. M. (2005). "Energetics in MRI Driven Turbulence," in *Magnetic Fields in the Universe: From Laboratory and Stars to Primordial Structures.* Editors E. M. de Gouveia dal Pino, G. Lugones and A. Lazarian

(Angra dos Reis: American Institute of Physics Conference Series), 475–488. doi:10.1063/1.2077209

Ginzburg, V. L., and Syrovatskii, S. I. (1965). Cosmic Magnetobremsstrahlung (Synchrotron Radiation). *Annu. Rev. Astron. Astrophys.* 3, 297–350. doi:10.1146/annurev.aa.03.090165.001501

Ginzburg, V. L. (1981). *Theoretical Physics and Astrophysics. Supplementary Chapters.* Moscow: Nauka.

Goldreich, P., and Sridhar, S. (1995). Toward a Theory of Interstellar Turbulence. 2: Strong Alfvenic Turbulence. *ApJ* 438, 763. doi:10.1086/175121

González-Casanova, D. F., and Lazarian, A. (2017). Velocity Gradients as a Tracer for Magnetic Fields. *ApJ* 835, 41. doi:10.3847/1538-4357/835/1/41

Guo, X., Mao, J., and Wang, J. (2017). Can Turbulence Dominate Depolarization of Optical Blazars? *ApJ* 843, 23. doi:10.3847/1538-4357/aa7385

Herron, C. A., Burkhart, B., Lazarian, A., Gaensler, B. M., and McClure-Griffiths, N. M. (2016). Radio Synchrotron Fluctuation Statistics as a Probe of Magnetized Interstellar Turbulence. *ApJ* 822, 13. doi:10.3847/0004-637X/822/1/13

Herron, C. A., Gaensler, B. M., Lewis, G. F., and McClure-Griffiths, N. M. (2018). Advanced Diagnostics for the Study of Linearly Polarized Emission. I. Derivation. *ApJ* 853, 9. doi:10.3847/1538-4357/aaa002

Ho, K. W., Yuen, K. H., Leung, P. K., and Lazarian, A. (2019). A Comparison between Faraday Tomography and Synchrotron Polarization Gradients. *ApJ* 887, 258. doi:10.3847/1538-4357/ab578c

Hu, Y., Xu, S., and Lazarian, A. (2021). Anisotropies in Compressible MHD Turbulence: Probing Magnetic Fields and Measuring Magnetization. *ApJ* 911, 37. doi:10.3847/1538-4357/abea18

Huang, Y.-M., and Bhattacharjee, A. (2016). Turbulent Magnetohydrodynamic Reconnection Mediated by the Plasmoid Instability. *ApJ* 818, 20. doi:10.3847/0004-637x/818/1/20

Iroshnikov, P. S. (1963). Turbulence of a Conducting Fluid in a Strong Magnetic Field. *Astronomicheskii Zhurnal* 40, 742.

Kandel, D., Lazarian, A., and Pogosyan, D. (2017a). Can the Observed E/B Ratio for Dust Galactic Foreground Be Explained by Sub-alfvénic Turbulence? *MNRAS* 472, L10–L14. doi:10.1093/mnrasl/slx128

Kandel, D., Lazarian, A., and Pogosyan, D. (2017b). Effects of Dust Absorption on Spectroscopic Studies of Turbulence. *MNRAS* 470, 3103–3123. doi:10.1093/mnras/stx1358

Kolmogorov, A. (1941). The Local Structure of Turbulence in Incompressible Viscous Fluid for Very Large Reynolds' Numbers. *Akademiia Nauk SSSR Doklady* 30, 301–305.

Kowal, G., Falceta-Gonçalves, D. A., Lazarian, A., and Vishniac, E. T. (2017). Statistics of Reconnection-Driven Turbulence. *ApJ* 838, 91. doi:10.3847/1538-4357/aa6001

Kowal, G., and Lazarian, A. (2010). Velocity Field of Compressible Magnetohydrodynamic Turbulence: Wavelet Decomposition and Mode Scalings. *ApJ* 720, 742–756. doi:10.1088/0004-637x/720/1/742

Kraichnan, R. H. (1965). Inertial-range Spectrum of Hydromagnetic Turbulence. *Phys. Fluids* 8, 1385–1387. doi:10.1063/1.1761412

Krall, N. A., Trivelpiece, A. W., and Gross, R. A. (1973). Principles of Plasma Physics. *Am. J. Phys.* 41, 1380–1381. doi:10.1119/1.1987587

Kunz, M. W., Stone, J. M., and Quataert, E. (2016). Magnetorotational Turbulence and Dynamo in a Collisionless Plasma. *Phys. Rev. Lett.* 117, 235101. doi:10.1103/physrevlett.117.235101

Lazarian, A. (2006). Enhancement and Suppression of Heat Transfer by MHD Turbulence. *ApJ* 645, L25–L28. doi:10.1086/505796

Lazarian, A., Eyink, G. L., Jafari, A., Kowal, G., Li, H., Xu, S., et al. (2020). 3D Turbulent Reconnection: Theory, Tests, and Astrophysical Implications. *Phys. Plasmas* 27, 012305. doi:10.1063/1.5110603

Lazarian, A., Pogosyan, D., and Esquivel, A. (2002). "Quest for H I Turbulence Statistics: New Techniques," in *Seeing through the Dust: The Detection of HI and the Exploration of the ISM in Galaxies.* Editors A. R. Taylor, T. L. Landecker and A. G. Willis (San Francisco: Astronomical Society of the Pacific Conference Series), 182.

Lazarian, A., and Pogosyan, D. (2016). Spectrum and Anisotropy of Turbulence from Multi-Frequency Measurement of Synchrotron Polarization. *ApJ* 818, 178. doi:10.3847/0004-637X/818/2/178

Lazarian, A., and Pogosyan, D. (2012). Statistical Description of Synchrotron Intensity Fluctuations: Studies of Astrophysical Magnetic Turbulence. *ApJ* 747, 5. doi:10.1088/0004-637x/747/1/5

Lazarian, A., and Pogosyan, D. (2004). Velocity Modification of the Power Spectrum from an Absorbing Medium. *ApJ* 616, 943–965. doi:10.1086/422462

Lazarian, A., and Vishniac, E. T. (1999). Reconnection in a Weakly Stochastic Field. *ApJ* 517, 700–718. doi:10.1086/307233

Lazarian, A., and Xu, S. (2021). Diffusion of Cosmic Rays in MHD Turbulence with Magnetic Mirrors. *ApJ* 923, 53. doi:10.3847/1538-4357/ac2de9

Lazarian, A., and Yuen, K. H. (2018a). Gradients of Synchrotron Polarization: Tracing 3d Distribution of Magnetic fields. *ApJ* 865, 59. doi:10.3847/1538-4357/aad3ca

Lazarian, A., Yuen, K. H., Ho, K. W., Chen, J., Lazarian, V., Lu, Z., et al. (2018b). Distribution of Velocity Gradient Orientations: Mapping Magnetization with the Velocity Gradient Technique. *ApJ* 865, 46. doi:10.3847/1538-4357/aad7ff

Lazarian, A., Yuen, K. H., Lee, H., and Cho, J. (2017). Synchrotron Intensity Gradients as Tracers of Interstellar Magnetic Fields. *ApJ* 842, 30. doi:10.3847/1538-4357/aa74c6

Lee, H., Cho, J., and Lazarian, A. (2019). Anisotropic Structure of Synchrotron Polarization. *ApJ* 877, 108. doi:10.3847/1538-4357/ab1b1e

Lee, H., Lazarian, A., and Cho, J. (2016). Polarimetric Studies of Magnetic Turbulence with an Interferometer. *ApJ* 831, 77. doi:10.3847/0004-637X/831/1/77

Loureiro, N. F., and Boldyrev, S. (2017). Role of Magnetic Reconnection in Magnetohydrodynamic Turbulence. *Phys. Rev. Lett.* 118, 245101. doi:10.1103/PhysRevLett.118.245101

Mac Low, M.-M., and Klessen, R. S. (2004). Control of star Formation by Supersonic Turbulence. *Rev. Mod. Phys.* 76, 125–194. doi:10.1103/RevModPhys.76.125

Mallet, A., and Schekochihin, A. A. (2017). A Statistical Model of Three-Dimensional Anisotropy and Intermittency in strong Alfvénic Turbulence. *Mon. Not. R. Astron. Soc.* 466, 3918–3927. doi:10.1093/mnras/stw3251

Mallet, A., Schekochihin, A. A., and Chandran, B. D. G. (2017). Disruption of Sheet-like Structures in Alfvénic Turbulence by Magnetic Reconnection. *MNRAS* 468, 4862–4871. doi:10.1093/mnras/stx670

Maron, J., and Goldreich, P. (2001). Simulations of Incompressible Magnetohydrodynamic Turbulence. *ApJ* 554, 1175–1196. doi:10.1086/321413

Mason, J., Cattaneo, F., and Boldyrev, S. (2006). Dynamic Alignment in Driven Magnetohydrodynamic Turbulence. *Phys. Rev. Lett.* 97, 255002. doi:10.1103/PhysRevLett.97.255002

McKee, C. F., and Ostriker, E. C. (2007). Theory of Star Formation. *Annu. Rev. Astron. Astrophys.* 45, 565–687. doi:10.1146/annurev.astro.45.051806.110602

Monin, A. S., and Yaglom, A. M. (1975). *Statistical Fluid Mechanics: Mechanics of Turbulence*. Cambridge: MIT Press.

Montgomery, D. (1982). Major Disruptions, Inverse Cascades, and the Strauss Equations. *Phys. Scr.* T2A, 83–88. doi:10.1088/0031-8949/1982/t2a/009

Ostriker, E. C. (2009). "ISM Theory: Gas Phases, Turbulence, and Star Formation," in *The Evolving ISM in the Milky Way and Nearby Galaxies*. Editors K. Sheth, A. Noriega-Crespo, J. G. Ingalls and R. Paladini 3 (Pasadena: The Fourth Spitzer Science Center Conference).

Quataert, E. (1998). Particle Heating by Alfvenic Turbulence in Hot Accretion Flows. *ApJ* 500, 978–991. doi:10.1086/305770

Reichherzer, P., Merten, L., Dörner, J., Becker Tjus, J., Pueschel, M. J., and Zweibel, E. G. (2022). Regimes of Cosmic-ray Diffusion in Galactic Turbulence. *SN Appl. Sci.* 4, 15. doi:10.1007/s42452-021-04891-z

Riols, A., Rincon, F., Cossu, C., Lesur, G., Ogilvie, G. I., and Longaretti, P.-Y. (2017). Magnetorotational Dynamo Chimeras. *A&A* 598, A87. doi:10.1051/0004-6361/201629285

Rybicki, G., and Lightman, A. (1979). Book-review-radiative Processes in Astrophysics. *Astron. Q.* 3, 199.

Schekochihin, A. A., Cowley, S. C., Dorland, W., Hammett, G. W., Howes, G. G., Quataert, E., et al. (2009). Astrophysical Gyrokinetics: Kinetic and Fluid Turbulent Cascades in Magnetized Weakly Collisional Plasmas. *ApJS* 182, 310–377. doi:10.1088/0067-0049/182/1/310

Sellwood, J. A., and Balbus, S. A. (1999). Differential Rotation and Turbulence in Extended HiDisks. *ApJ* 511, 660–665. doi:10.1086/306728

Shebalin, J. V., Matthaeus, W. H., and Montgomery, D. (1983). Anisotropy in Mhd Turbulence Due to a Mean Magnetic Field. *J. Plasma Phys.* 29, 525–547. doi:10.1017/s0022377800000933

Spitzer Jr, L. (1978). Review of Publications: Physical Processes in the Interstellar Medium. *J. R. Astronomical Soc. Can.* 72, 349.

Stutzki, J., Bensch, F., Heithausen, A., Ossenkopf, V., and Zielinsky, M. (1998). On the Fractal Structure of Molecular Clouds. *A&A* 336, 697–720.

Subramanian, K., Shukurov, A., and Haugen, N. E. L. (2006). Evolving Turbulence and Magnetic fields in Galaxy Clusters. *Monthly Notices R. Astronomical Soc.* 366, 1437–1454. doi:10.1111/j.1365-2966.2006.09918.x

Taylor, A. R., Gibson, S. J., Peracaula, M., Martin, P. G., Landecker, T. L., Brunt, C. M., et al. (2003). The Canadian Galactic Plane Survey. *Astron. J.* 125, 3145–3164. doi:10.1086/375301

Vasquez, B. J., Isenberg, P. A., and Markovskii, S. A. (2020). Proton Perpendicular Heating in Turbulence Simulations: Determination of the Velocity Diffusion Coefficient. *ApJ* 893, 71. doi:10.3847/1538-4357/ab7e2b

Waelkens, A. H., Schekochihin, A. A., and Enßlin, T. A. (2009). Probing Magnetic Turbulence by Synchrotron Polarimetry: Statistics and Structure of Magnetic fields from Stokes Correlators. *MNRAS* 398, 1970–1988. doi:10.1111/j.1365-2966.2009.15231.x

Wang, R.-Y., Zhang, J.-F., Lazarian, A., Xiao, H.-P., and Xiang, F.-Y. (2021). Gradient Measurement of Synchrotron Polarization Diagnostic: Application to Spatially Separated Emission and Faraday Rotation Regions. *MNRAS* 505, 6206–6216. doi:10.1093/mnras/stab1708

Wang, R.-Y., Zhang, J.-F., and Xiang, F.-Y. (2020). Studying the Anisotropy of Compressible Magnetohydrodynamic Turbulence by Synchrotron Polarization Intensity. *ApJ* 890, 70. doi:10.3847/1538-4357/ab6a1a

Wang, T., He, J., Alexandrova, O., Dunlop, M., and Perrone, D. (2020). Observational Quantification of Three-Dimensional Anisotropies and Scalings of Space Plasma Turbulence at Kinetic Scales. *ApJ* 898, 91. doi:10.3847/1538-4357/ab99ca

Wicks, R. T., Mallet, A., Horbury, T. S., Chen, C. H., Schekochihin, A. A., and Mitchell, J. J. (2013). Alignment and Scaling of Large-Scale Fluctuations in the Solar Wind. *Phys. Rev. Lett.* 110, 025003. doi:10.1103/PhysRevLett.110.025003

Xu, S., and Hu, Y. (2021). Measuring Magnetization with Rotation Measures and Velocity Centroids in Supersonic MHD Turbulence. *ApJ* 910, 88. doi:10.3847/1538-4357/abe403

Xu, S., and Lazarian, A. (2018). Resonance-broadened Transit Time Damping of Particles in MHD Turbulence. *ApJ* 868, 36. doi:10.3847/1538-4357/aae840

Yan, H., and Lazarian, A. (2008). Cosmic-Ray Propagation: Nonlinear Diffusion Parallel and Perpendicular to Mean Magnetic Field. *ApJ* 673, 942–953. doi:10.1086/524771

Yang, B., Zhang, J.-F., Lazarian, A., and de Medeiros, J. R. (2021). Statistical Tracing of Turbulent Magnetic fields in the Optically Thick Interstellar Medium. *MNRAS* 503, 768–776. doi:10.1093/mnras/stab236

Yang, R., Aharonian, F., and Evoli, C. (2016). Radial Distribution of the Diffuseγ-ray Emissivity in the Galactic Disk. *Phys. Rev. D* 93, 123007. doi:10.1103/physrevd.93.123007

Yuan, F., Gan, Z., Narayan, R., Sadowski, A., Bu, D., and Bai, X.-N. (2015). Numerical Simulation of Hot Accretion Flows. III. Revisiting Wind Properties Using the Trajectory Approach. *ApJ* 804, 101. doi:10.1088/0004-637X/804/2/101

Yuen, K. H., and Lazarian, A. (2017). Tracing Interstellar Magnetic Field Using Velocity Gradient Technique: Application to Atomic Hydrogen Data. *ApJ* 837, L24. doi:10.3847/2041-8213/aa6255

Zhang, J.-F., Hu, K., Cho, J., and Lazarian, A. (2020). Studying the Local Magnetic Field and Anisotropy of Magnetic Turbulence by Synchrotron Polarization Derivative. *ApJ* 895, 20. doi:10.3847/1538-4357/ab88ac

Zhang, J.-F., Lazarian, A., Ho, K. W., Yuen, K. H., Yang, B., and Hu, Y. (2019a). Tracing Magnetic Field with Synchrotron Polarization Gradients: Parameter Study. *MNRAS* 486, 4813–4822. doi:10.1093/mnras/stz1176

Zhang, J.-F., Lazarian, A., Lee, H., and Cho, J. (2016). Studying Magnetohydrodynamic Turbulence with Synchrotron Polarization Dispersion. *ApJ* 825, 154. doi:10.3847/0004-637x/825/2/154

Zhang, J.-F., Lazarian, A., and Xiang, F.-Y. (2018). Spectral Properties of Magnetohydrodynamic Turbulence Revealed by Polarization Synchrotron Emission with Faraday Rotation. *ApJ* 863, 197. doi:10.3847/1538-4357/aad182

Zhang, J.-F., Liu, Q., and Lazarian, A. (2019b). Tracing Magnetic Fields by the Synergies of Synchrotron Emission Gradients. *ApJ* 886, 63. doi:10.3847/1538-4357/ab4b4a

Zhang, J.-F., and Xiang, F.-Y. (2021). Energetic Particle Acceleration in Compressible Magnetohydrodynamic Turbulence. *ApJ* 922, 209. doi:10.3847/1538-4357/ac28ff

Zhdankin, V., Uzdensky, D. A., Werner, G. R., and Begelman, M. C. (2019). Electron and Ion Energization in Relativistic Plasma Turbulence. *Phys. Rev. Lett.* 122, 055101. doi:10.1103/PhysRevLett.122.055101

Zhdankin, V., Walker, J., Boldyrev, S., and Lesur, G. (2017). Universal Small-Scale Structure in Turbulence Driven by Magnetorotational Instability. *MNRAS* 467, 3620–3627. doi:10.1093/mnras/stx372

Zhuravleva, I., Churazov, E., Schekochihin, A. A., Allen, S. W., Vikhlinin, A., and Werner, N. (2019). Suppressed Effective Viscosity in the Bulk Intergalactic Plasma. *Nat. Astron.* 3, 832–837. doi:10.1038/s41550-019-0794-z

Zucca, A., Li, Y., and Pogosian, L. (2017). Constraints on Primordial Magnetic fields from Planck Data Combined with the South Pole Telescope CMB B -mode Polarization Measurements. *Phys. Rev. D* 95, 063506. doi:10.1103/physrevd.95.063506